

See discussions, stats, and author profiles for this publication at: <https://www.researchgate.net/publication/288109862>

An overview of tight-binding method for two-dimensional carbon structures

Chapter · January 2012

CITATIONS

8

READS

1,111

2 authors, including:



Sina Khorasani

University of Vienna

186 PUBLICATIONS 962 CITATIONS

[SEE PROFILE](#)

Some of the authors of this publication are also working on these related projects:



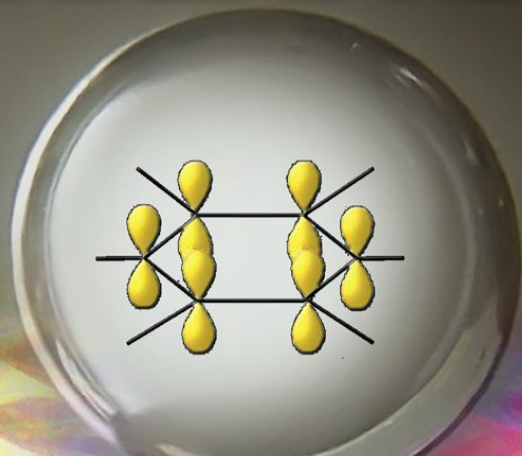
Physical Optics [View project](#)



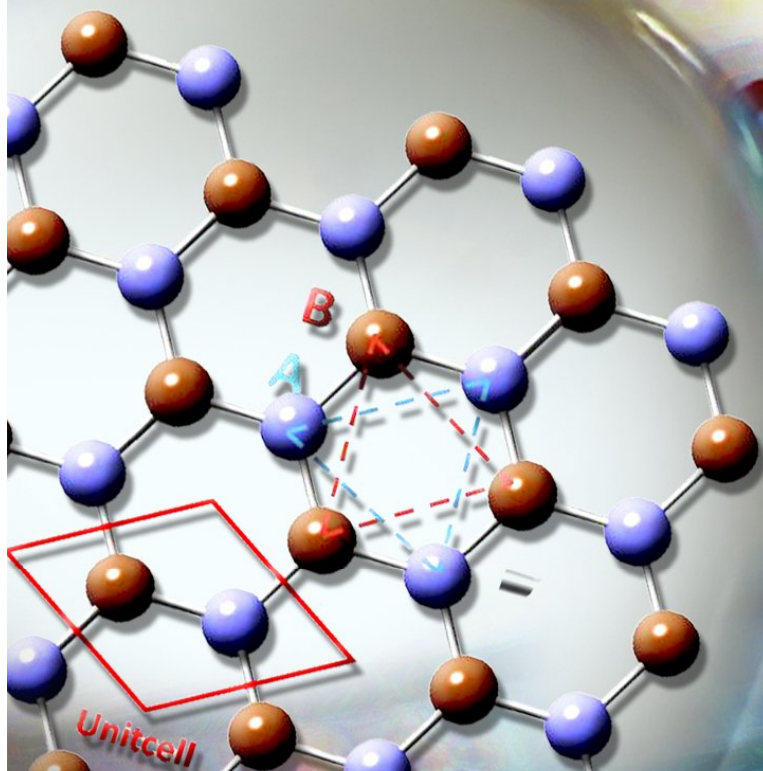
2D Materials [View project](#)

GRAPHENE

Properties,
Synthesis and
Applications



Zhiping Xu
Editor



Nanotechnology Science and Technology

NOVA

Chapter 1

AN OVERVIEW OF TIGHT-BINDING METHOD FOR TWO-DIMENSIONAL CARBON STRUCTURES

Behnaz Gharekhanlou and Sina Khorasani*

School of Electrical Engineering
Sharif University of Technology
P. O. Box 11365-9363, Tehran
Iran

Abstract

Since the advent of graphene, the two-dimension allotrope of carbon, there has been a growing interest in calculation of quantum mechanical properties of this crystal and its derivatives. To this end, the tight-binding model has been in frequent use for a relatively long period of time. This review, presents an in-depth survey on this method as possible to graphene and two of the most important related structures, graphene anti-dot lattice, and graphane. The two latter derivatives of graphene are semiconducting, while graphane is semimetallic. We present band structure and quantum mechanical orbital calculations and justify the results with the density function theory.

Key words: Graphene, Graphane, Carbon Nanostructures, Tight-binding Method, Quantum Mechanics.

I. TIGHT-BINDING METHOD

I.1. Introduction

The tight-binding model (or TB model) is an approach to the calculation of electronic band structure using an approximate set of wave functions based upon superposition of wave

* E-mail address: khorasani@sina.sharif.edu

functions for isolated atoms located at each atomic site. This model describes the properties of tightly bound electrons in solids. The electrons in this model should be tightly bound to the atom to which they belong and they should have limited interaction with states and potentials on surrounding atoms of the solid. As a result the wave function of the electron will be rather similar to the atomic orbital of the free atom where it belongs to. This method was developed by Bloch [1] in 1928 considered only the satomc orbital. In 1934 Jones, Mott, and Skinner [2] considered different atomic orbitals.

Tight-binding models are applied to a wide variety of solids. The model gives good qualitative results in many cases and can be combined with other models that give better results where the tight-binding model fails. Though the tight-binding approach is a one-electron model, it also provides a basis for more advanced calculations like the calculation of surface states and application to various kinds of many-body problem and quasiparticle calculations. It is also a common practice to use optimized tight-binding methods, in which the values of the matrix elements are derived approximately or fitted to experiment or other theories [3].

I.2. Secular Equation

In a crystalline solid, the translational symmetry along the directions of the lattice vectors \mathbf{a}_i , enforces the Bloch's theorem to be satisfied by any wave function of the lattice. Mathematically, this can be written as

$$\mathbb{T}\psi_k(r) = e^{i\mathbf{k}\cdot\mathbf{a}_i} \psi_k(r) \quad (i = 1, 2, 3), \quad (1)$$

where \mathbb{T} is the translation operator along the lattice vector \mathbf{a}_i , and \mathbf{k} is the Bloch wave vector [4, 5]. In the tight-binding model of electronic structures, single electron wave functions are normally expanded in terms of atomic orbitals [6, 7]

$$\varphi_{nlm}(r, \theta, \Phi) = R_{nl}(r)Y_{lm}(\theta, \Phi), \quad (2)$$

where R_{nl} and Y_{lm} are radial and spherical-harmonic functions in polar coordinates and n , l , and m are the principal, angular-momentum, and magnetic quantum numbers, respectively.

The wave function can be defined in variety of models, but the most commonly used form is a linear combination of atomic orbitals. Thus the wave function $\phi(\mathbf{k}, \mathbf{r})$ is defined as a summation on the atomic wavefunction $\varphi(\mathbf{r} - \mathbf{R}_j)$ on the site j

$$\phi_j(\mathbf{k}, \mathbf{r}) = \frac{1}{\sqrt{N}} \sum_{\mathbf{R}_j}^N e^{i\mathbf{k}\cdot\mathbf{R}_j} \varphi(\mathbf{r} - \mathbf{R}_j) \quad (j = 1, \dots, n), \quad (3)$$

where \mathbf{R}_j is the position of the atom and N is the number of atomic wavefunctions in the unit cell. It is easy to verify that this function satisfies Bloch condition

$$\begin{aligned}
 \phi_j(\mathbf{k}, \mathbf{r} + \mathbf{a}) &= \frac{1}{\sqrt{N}} \sum_{\mathbf{R}_j}^N e^{i \mathbf{k} \cdot \mathbf{R}_j} \varphi(\mathbf{r} + \mathbf{a} - \mathbf{R}_j) \\
 &= e^{i \mathbf{k} \cdot \mathbf{a}_j} \frac{1}{\sqrt{N}} \sum_{\mathbf{R}_j - \mathbf{a}}^N e^{i \mathbf{k} \cdot (\mathbf{R}_j - \mathbf{a})} \varphi[\mathbf{r} - (\mathbf{R}_j - \mathbf{a})] \\
 &= e^{i \mathbf{k} \cdot \mathbf{a}_j} \phi_j(\mathbf{k}, \mathbf{r}).
 \end{aligned} \tag{4}$$

In a solid, eigenfunctions $\psi_j(\mathbf{k}, \mathbf{r})$ ($j = 1, \dots, n$) are defined as a linear recombination of Bloch functions

$$\psi_j(\mathbf{k}, \mathbf{r}) = \sum_{j'=1}^n C_{jj'}(\mathbf{k}) \phi_j(\mathbf{k}, \mathbf{r}). \tag{5}$$

Here, $C_{jj'}(\mathbf{k})$ are coefficients which have to be determined.

The eigenvalues of the system described by the Hamiltonian \mathbb{H} is given by [8]

$$E_j(\mathbf{k}) = \frac{\langle \psi_j | \mathbb{H} | \psi_j \rangle}{\langle \psi_j | \psi_j \rangle} = \frac{\int \psi_j^*(\mathbf{k}, \mathbf{r}) \mathbb{H} \psi_j(\mathbf{k}, \mathbf{r}) dr}{\int \psi_j^*(\mathbf{k}, \mathbf{r}) \psi_j(\mathbf{k}, \mathbf{r}) dr}. \tag{6}$$

Now, substituting $\psi_j(\mathbf{k}, \mathbf{r})$ as defined in (5) leads to

$$\begin{aligned}
 E_j(\mathbf{k}) &= \frac{\sum_{j,j'=1}^n C_{ij}^* C_{ij'} \langle \phi_j | \mathbb{H} | \phi_{j'} \rangle}{\sum_{j,j'=1}^n C_{ij}^* C_{ij'} \langle \phi_j | \phi_{j'} \rangle} = \frac{\sum_{j,j'=1}^n H_{jj'}(\mathbf{k}) C_{ij}^* C_{ij'}}{\sum_{j,j'=1}^n S_{jj'}(\mathbf{k}) C_{ij}^* C_{ij'}},
 \end{aligned} \tag{7}$$

where $H_{jj'}(\mathbf{k})$ and $S_{jj'}(\mathbf{k})$ are transfer and overlap matrices, respectively, and are defined by

$$H_{jj'}(\mathbf{k}) = \langle \phi_j | \mathbb{H} | \phi_{j'} \rangle, \tag{8}$$

$$S_{jj'}(\mathbf{k}) = \langle \phi_j | \phi_{j'} \rangle. \tag{9}$$

For a given \mathbf{k} value, the coefficient $C_{jj'}^*(\mathbf{k})$ is optimized so as to minimize $E_i(\mathbf{k})$

$$\begin{aligned}
 \frac{\partial E_i(\mathbf{k})}{\partial C_{ij}^*(\mathbf{k})} &= \frac{\sum_{j'=1}^n H_{jj'}(\mathbf{k}) C_{ij'}(\mathbf{k})}{\sum_{j,j'=1}^n S_{jj'}(\mathbf{k}) C_{ij}^*(\mathbf{k}) C_{ij'}(\mathbf{k})} \\
 &\quad - \frac{\sum_{j,j'=1}^n H_{jj'}(\mathbf{k}) C_{ij}^*(\mathbf{k}) C_{ij'}(\mathbf{k})}{\left[\sum_{j,j'=1}^n S_{jj'}(\mathbf{k}) C_{ij}^*(\mathbf{k}) C_{ij'}(\mathbf{k}) \right]^2} \sum_{j'=1}^n S_{jj'}(\mathbf{k}) C_{ij'}(\mathbf{k}) = 0.
 \end{aligned} \tag{10}$$

This further can be rewritten as

$$\frac{\sum_{j'=1}^n H_{jj'}(\mathbf{k}) C_{ij'}(\mathbf{k})}{\sum_{j,j'=1}^n S_{jj'}(\mathbf{k}) C_{ij}^*(\mathbf{k}) C_{ij'}(\mathbf{k})} - \left[\frac{\sum_{j,j'=1}^n H_{jj'}(\mathbf{k}) C_{ij}^*(\mathbf{k}) C_{ij'}(\mathbf{k})}{\sum_{j,j'=1}^n S_{jj'}(\mathbf{k}) C_{ij}^*(\mathbf{k}) C_{ij'}(\mathbf{k})} \right] \frac{\sum_{j'=1}^n S_{jj'}(\mathbf{k}) C_{ij'}(\mathbf{k})}{\sum_{j,j'=1}^n S_{jj'}(\mathbf{k}) C_{ij}^*(\mathbf{k}) C_{ij'}(\mathbf{k})} = 0. \quad (11)$$

This in turn can be readily simplified as

$$\sum_{j'=1}^n H_{jj'}(\mathbf{k}) C_{ij'}(\mathbf{k}) - E_i(\mathbf{k}) \sum_{j'=1}^n S_{jj'}(\mathbf{k}) C_{ij'}(\mathbf{k}) = 0. \quad (12)$$

Putting in the matrix form we get

$$\{[\mathbf{H}] - E_i(\mathbf{k})[\mathbf{S}]\}\{C_i(\mathbf{k})\} = 0. \quad (13)$$

If the matrix $[\mathbf{H}] - E_i(\mathbf{k})[\mathbf{S}]$ has an inverse, the vector $\{C_i(\mathbf{k})\}$ will be identically zero and this leads to the trivial solution. Thus, non-trivial solutions require

$$\|[\mathbf{H}] - E_i(\mathbf{k})[\mathbf{S}]\| = 0. \quad (14)$$

This equation is called the secular equation, whose eigenvalues $E_i(\mathbf{k})$ give the energy bandstructure.

As an example, suppose that the primitive basis contains one atom with the atomic orbital function $\varphi(\mathbf{r})$. We get

$$\phi_j(\mathbf{k}, \mathbf{r}) = \frac{1}{\sqrt{N}} \sum_{\mathbf{R}_j}^N e^{i\mathbf{k}\cdot\mathbf{R}_j} \varphi(\mathbf{r} - \mathbf{R}_j) \quad (j = 1, \dots, n). \quad (15)$$

Here we use the nearest-neighbor Hamiltonian of the system; it means that only the effect of the nearest-neighbors of the atom in the unit cell is considered. The transfer and overlap matrices are now defined respectively as follows

$$\begin{aligned} H_{jj}(\mathbf{k}) &= \langle \phi_j | \mathbb{H} | \phi_j \rangle = \frac{1}{N} \sum_{\mathbf{R}_j}^N \sum_{\mathbf{R}'_j}^N e^{i\mathbf{k}\cdot(\mathbf{R}_j - \mathbf{R}'_j)} \langle \varphi(\mathbf{r} - \mathbf{R}_j) | \mathbb{H} | \varphi(\mathbf{r} - \mathbf{R}'_j) \rangle \\ &= \frac{1}{N} \sum_{\mathbf{R}_j = \mathbf{R}'_j}^N \langle \varphi(\mathbf{r} - \mathbf{R}_j) | \mathbb{H} | \varphi(\mathbf{r} - \mathbf{R}_j) \rangle \\ &\quad + \frac{1}{N} \sum_{\mathbf{R}'_j = \mathbf{R}_j + \mathbf{a}}^N e^{i\mathbf{k}\cdot\mathbf{a}} \langle \varphi(\mathbf{r} - \mathbf{R}_j) | \mathbb{H} | \varphi[\mathbf{r} - (\mathbf{R}_j + \mathbf{a})] \rangle + \dots \\ &= -\alpha - \gamma_0 \sum_{\mathbf{R}'_j = \mathbf{R}_j + \mathbf{a}}^N e^{i\mathbf{k}\cdot\mathbf{a}} \end{aligned} \quad (16)$$

$$\begin{aligned}
S_{jj}(\mathbf{k}) &= \langle \phi_j | \phi_j \rangle = \frac{1}{N} \sum_{\mathbf{R}_j}^N \sum_{\mathbf{R}'_j} e^{i\mathbf{k}\cdot(\mathbf{R}_j - \mathbf{R}'_j)} \langle \varphi(\mathbf{r} - \mathbf{R}_j) | \varphi(\mathbf{r} - \mathbf{R}'_j) \rangle \\
&= \frac{1}{N} \sum_{\substack{\mathbf{R}_j = \mathbf{R}'_j}}^N \langle \varphi(\mathbf{r} - \mathbf{R}_j) | \varphi(\mathbf{r} - \mathbf{R}_j) \rangle \\
&\quad + \frac{1}{N} \sum_{\substack{\mathbf{R}'_j = \mathbf{R}_j + \mathbf{a}}}^N e^{i\mathbf{k}\cdot\mathbf{a}} \langle \varphi(\mathbf{r} - \mathbf{R}_j) | \varphi[\mathbf{r} - (\mathbf{R}_j + \mathbf{a})] \rangle + \dots = 1.
\end{aligned} \tag{17}$$

Here, we assume that the atomic wavefunction is normalized. Then, the secular equation reduces to

$$E(\mathbf{k}) = -\alpha - \gamma_0 \sum_{\substack{\mathbf{R}'_j = \mathbf{R}_j + \mathbf{a}}}^N e^{i\mathbf{k}\cdot\mathbf{a}}. \tag{18}$$

The constant parameters α and γ_0 are usually found by fitting this equation to high symmetric points of experimental data.

We can use an important approximation in the Tight-binding method, when considering the orbital number l , as well. One can rewrite (3) as

$$\phi_{li}(\mathbf{k}, \mathbf{r}) = \frac{1}{\sqrt{N}} \sum_{\mathbf{R}} e^{i\mathbf{k}\cdot\mathbf{R}} \varphi(\mathbf{r} - \mathbf{t}_i - \mathbf{R}). \tag{19}$$

The corresponding eigenfunction would be given by

$$\psi(\mathbf{k}, \mathbf{r}) = \sum_{l,i}^n C_{li}(\mathbf{k}) \phi_{li}(\mathbf{k}, \mathbf{r}). \tag{20}$$

Hence, the Schrödinger Hamiltonian equation takes the form

$$\mathbf{H}\psi = E\psi,$$

$$\sum_{l,i} \left[\langle \phi_{mj}(\mathbf{k}, \mathbf{r}) | \mathbb{H} | \phi_{li}(\mathbf{k}, \mathbf{r}) \rangle - E(\mathbf{k}) \langle \phi_{mj}(\mathbf{k}, \mathbf{r}) | \phi_{li}(\mathbf{k}, \mathbf{r}) \rangle \right] C_{li}(\mathbf{k}) = 0. \tag{21}$$

In order to solve this linear system we need to be able to evaluate the following parameters:

$$\begin{aligned}
\langle \phi_{mj}(\mathbf{k}, \mathbf{r}) | \phi_{li}(\mathbf{k}, \mathbf{r}) \rangle &= \frac{1}{N} \sum_{\mathbf{R}} e^{i\mathbf{k}\cdot\mathbf{R}} \langle \varphi_m(\mathbf{r} - \mathbf{t}_j) | \varphi_l(\mathbf{r} - \mathbf{t}_i - \mathbf{R}) \rangle \\
&= \sum_{\mathbf{R}}^N e^{i\mathbf{k}\cdot\mathbf{R}} \langle \varphi_m(\mathbf{r} - \mathbf{t}_j) | \varphi_l(\mathbf{r} - \mathbf{t}_i - \mathbf{R}) \rangle.
\end{aligned} \tag{22}$$

In a similar way, we have

$$\begin{aligned}
\langle \phi_{mj}(\mathbf{k}, \mathbf{r}) | \mathbb{H} | \phi_{li}(\mathbf{k}, \mathbf{r}) \rangle &= \frac{1}{N} \sum_{\mathbf{R}} e^{i\mathbf{k}\cdot\mathbf{R}} \langle \varphi_m(\mathbf{r} - \mathbf{t}_j) | \mathbb{H} | \varphi_l(\mathbf{r} - \mathbf{t}_i - \mathbf{R}) \rangle \\
&= \sum_{\mathbf{R}}^N e^{i\mathbf{k}\cdot\mathbf{R}} \langle \varphi_m(\mathbf{r} - \mathbf{t}_j) | \mathbb{H} | \varphi_l(\mathbf{r} - \mathbf{t}_i - \mathbf{R}) \rangle.
\end{aligned} \tag{23}$$

At this point we can use an important approximation [11]: the overlap matrix elements in (9) is non-zero only for the same orbitals on the same atom, i.e.

$$\langle \varphi_m(\mathbf{r} - \mathbf{t}_j) | \varphi_l(\mathbf{r} - \mathbf{t}_i - \mathbf{R}) \rangle = \delta_{lm} \delta_{ij} \delta(\mathbf{R}). \quad (24)$$

This is referred to as an “orthogonal basis”, since any overlap between different orbitals on the same atom or orbitals on different atoms is taken to be zero. So it will be a unit matrix.

Similarly, we will take the Hamiltonian matrix elements in (8) to be non-zero only if the orbitals are on the same atom which are referred to as the “on-site energies”:

$$\langle \varphi_m(\mathbf{r} - \mathbf{t}_j) | \mathbb{H} | \varphi_l(\mathbf{r} - \mathbf{t}_i - \mathbf{R}) \rangle = \delta_{lm} \delta_{ij} \delta(\mathbf{R}) \varepsilon_l. \quad (25)$$

The above relation implies that if the orbitals belong to different atoms, but situated at nearest neighbor sites, denoted in general as \mathbf{d} , one would get the following

$$\langle \varphi_m(\mathbf{r} - \mathbf{t}_j) | \mathbb{H} | \varphi_l(\mathbf{r} - \mathbf{t}_i - \mathbf{R}) \rangle = \delta(\mathbf{t}_j - \mathbf{t}_i - \mathbf{R} - \mathbf{d}) V_{lm,ij}. \quad (26)$$

The $V_{lm,ij}$ are also referred to as “hopping” matrix elements.

Now, one needs only to find the on-site and hopping matrix elements, from which the energy eigenvalues of the related Hamiltonian matrix are found.

II. CARBON ATOM

II.1. Introduction

Carbon is present in nature in many allotropic forms like graphite, diamond, fullerenes, nanotubes, etc. This is because of the versatility of its bonding. Carbon is the sixth element of the periodic table. Each carbon atom has six electrons in the configuration $1s^2$, $2s^2$, and $2p^2$ atomic orbitals, i.e. 2 electrons fill the inner shell $1s$, which is close to the nucleus and which is irrelevant for chemical reactions, whereas 4 electrons occupy the outer shell of $2s$ and $2p$ orbitals. Because of low difference in energy of $2s$ and $2p$ levels in carbon, the electronic wave functions for these four electrons can be mixed with each other, changing the occupation of the $2s$ and three $2p$ atomic orbitals so as to enhance the binding energy of the C atom with its neighboring atoms [8, 9]. These orbitals are called hybrid orbitals. In carbon, mixing of $2s$ and $2p$ orbitals leads to three possible hybridizations sp , sp^2 and sp^3 , generally called sp^n hybridization with $n = 1, 2, 3$. Other elements of this group such as Si, Ge exhibit sp^3 hybridization. Carbon differs from Si and Ge because it only has the spherical $1s$ orbitals as inner atomic orbitals so that the absence of nearby inner orbitals facilitates hybridizations involving only valence s and p orbitals for carbon. The lack of sp and sp^2 hybridization in Si and Ge might be related to the absence of “organic materials” made of Si and Ge [8].

II.2. Hybridization in Carbon Allotropes

II.2.1. sp Hybrid Orbitals

The sp hybrid atomic orbitals are one of the possible states of electron in an atom, especially when it is bonded to others. These electron states have half $2s$ and half $2p$ characters. We can see this kind of hybridization in chemical compounds such as ethyne. This type of hybridization has been also recently observed in free carbon nanoparticles [10].

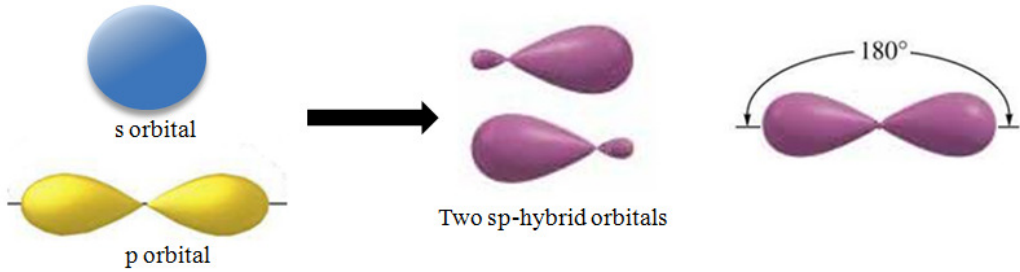


Figure II.2.1. sp hybridization.

For illustration, we choose the $|2p_x\rangle$ state. From a mathematical view point, there are two ways to combine the 2s and 2p atomic orbitals, obtained by the symmetric and anti-symmetric combinations

$$\begin{aligned} |sp_+\rangle &= C_1|2s\rangle + C_2|2p_x\rangle, \\ |sp_-\rangle &= C_3|2s\rangle + C_4|2p_x\rangle. \end{aligned} \quad (27)$$

Using the ortho-normality conditions $\langle sp_+|sp_-\rangle = 0$, $\langle sp_+|sp_+\rangle = 1$, and $\langle sp_-|sp_-\rangle = 1$, the relationships between the coefficients are obtained as follow

$$\begin{aligned} C_1C_3 + C_2C_4 &= 0, & C_1^2 + C_2^2 &= 1, \\ C_3^2 + C_4^2 &= 1, & C_1^2 + C_3^2 &= 1. \end{aligned} \quad (28)$$

The result is

$$\begin{aligned} |sp_+\rangle &= \frac{1}{\sqrt{2}}(|2s\rangle + |2p_x\rangle), \\ |sp_-\rangle &= \frac{1}{\sqrt{2}}(|2s\rangle - |2p_x\rangle). \end{aligned} \quad (29)$$

These energy states have a region of high electron probability each, and the two atomic orbitals are located opposite to each other, centered on the atom.

II.2.2. sp^2 Hybrid Orbitals

If we mix two of the 2p orbitals with a 2s orbital, we end up with three sp^2 hybridized orbitals. In the case of a superposition of the 2s and two 2p orbitals, which we maychoose to be the $|2p_x\rangle$ and the $|2p_y\rangle$ states, one obtains the planar sp^2 hybridization. These three orbitals lie on a plane and make equal angles of 120° , pointing to the vertices of an equilateral triangle. When the central atom makes use of sp^2 hybridized orbitals, the compound so formed has a trigonal shape as shown in Figure II.2.2.

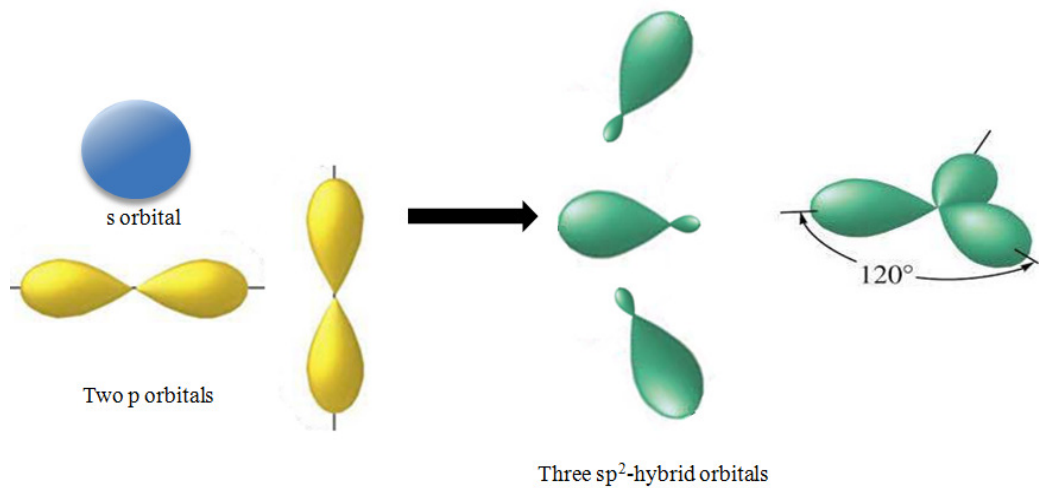


Figure II.2.2. sp^2 hybridization.

From a mathematical view point we have

$$\begin{aligned} |sp_1^2\rangle &= C_1 |2s\rangle - \sqrt{1-C_1^2} |2p_y\rangle, \\ |sp_2^2\rangle &= C_2 |2s\rangle + \sqrt{1-C_2^2} \left\{ \frac{\sqrt{3}}{2} |2p_x\rangle + \frac{1}{2} |2p_y\rangle \right\}, \\ |sp_3^2\rangle &= C_3 |2s\rangle + \sqrt{1-C_3^2} \left\{ -\frac{\sqrt{3}}{2} |2p_x\rangle + \frac{1}{2} |2p_y\rangle \right\}. \end{aligned} \quad (30)$$

Using ortho-normality conditions, we obtain

$$\begin{aligned} C_1^2 + C_2^2 + C_3^2 &= 1 \\ C_1 C_2 - \frac{1}{2} \sqrt{1-C_1^2} \sqrt{1-C_2^2} &= 0 \quad \Rightarrow \quad C_1 = C_2 = \frac{1}{\sqrt{3}}, \quad C_3 = -\frac{1}{\sqrt{3}}. \\ C_1 C_3 - \frac{1}{2} \sqrt{1-C_1^2} \sqrt{1-C_3^2} &= 0 \end{aligned} \quad (31)$$

Hence, the three possible quantum-mechanical states are given by

$$\begin{aligned} |sp_1^2\rangle &= \frac{1}{\sqrt{3}} |2s\rangle - \sqrt{\frac{2}{3}} |2p_y\rangle, \\ |sp_2^2\rangle &= \frac{1}{\sqrt{3}} |2s\rangle + \sqrt{\frac{2}{3}} \left\{ \frac{\sqrt{3}}{2} |2p_x\rangle + \frac{1}{2} |2p_y\rangle \right\}, \\ |sp_3^2\rangle &= -\frac{1}{\sqrt{3}} |2s\rangle + \sqrt{\frac{2}{3}} \left\{ -\frac{\sqrt{3}}{2} |2p_x\rangle + \frac{1}{2} |2p_y\rangle \right\}. \end{aligned} \quad (32)$$

When carbon atoms make use of sp^2 hybrid orbitals for σ bonding, the three bonds lie on the same plane. Such carbon allotropes include the two-dimensional graphite and graphene, the one-dimensional carbon nanotube, and the zero-dimensional fullerene, in which, every

pair of carbon atoms make use of sp^2 hybrid orbitals. The remaining p orbitals of carbon atoms overlap to form a π bond.

π bonds result from the overlap of atomic orbitals that are in contact through two areas of overlap. π bonds are more diffuse bonds than the σ bonds. Electrons in π bonds are sometimes referred to as π electrons.

In the case of sp^2 hybridization, the carbon atom is a special case. Because the only orbital bonded to the nucleus is 1s, the size of atoms is small and the resultant band is considerably strong. Other elements of group IV normally appear in sp^3 hybridization. Going down the table of periodic element of this group, and with the physical size of the elements increasing, the bond energy is reduced, and eventually the last element of this group, that is Pb, becomes a metal rather than being a semiconductor. Since the π bonds are much weaker than σ bonds, forming of π bonds in the other elements of this group would be highly unstable. While the bonding energy of π orbitals in Si is only about 25Kcalmol^{-1} , this value is about 60Kcalmol^{-1} for carbon.

II.2.3. sp^3 Hybrid Orbitals

Carbon atoms in diamond provide a simple example of sp^3 hybrid orbitals. Mixing one s and all three p atomic orbitals produces a set of four equivalent sp^3 hybrid atomic orbitals. When carbon atoms make use of sp^3 hybrid orbitals, the four bonds around each carbon atom point toward the vertices of a regular tetrahedron and make angles of 109.5° .

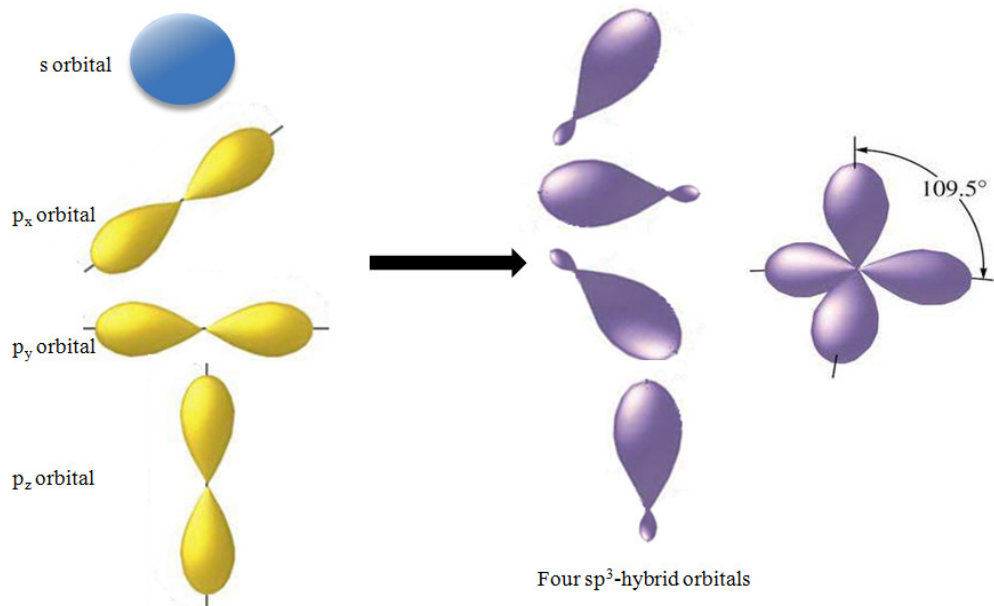


Figure II.2.3. sp^3 hybridization.

Using calculations similar to previous sections, four sp^3 hybrid orbitals are given by

$$\begin{aligned}
 |sp_1^3\rangle &= \frac{1}{2}\{|2s\rangle + |2p_x\rangle + |2p_y\rangle + |2p_z\rangle\}, \\
 |sp_2^3\rangle &= \frac{1}{2}\{|2s\rangle - |2p_x\rangle - |2p_y\rangle + |2p_z\rangle\}, \\
 |sp_3^3\rangle &= \frac{1}{2}\{|2s\rangle - |2p_x\rangle + |2p_y\rangle - |2p_z\rangle\}, \\
 |sp_4^3\rangle &= \frac{1}{2}\{|2s\rangle + |2p_x\rangle - |2p_y\rangle - |2p_z\rangle\}.
 \end{aligned} \tag{33}$$

When sp^3 hybrid orbitals are used for the central atom in the formation of molecule, the molecule is said to have the shape of a tetrahedron.

In general for sp^n hybridization, $n+1$ electrons belong to the carbon atom occupied in the hybridized σ orbital and $4-(n+1)$ electrons remain in the π orbital.

III.3. Vanishing and Non-vanishing Orbital Interactions Based on TB model

To study carbon allotrops, there are four atomic orbitals per atom: one s-type and three p-type (p_x, p_y, p_z). We want to use Tight-binding method to obtain the electronic band structure. Therefore we work within the orthogonal basis of orbitals and nearest neighbor interactions only, as described by the equations of (14). To solve this eigenvalue problem we need the Hamiltonian matrix elements between these atomic orbitals at different interatomic distance. For the sp-bonding, there are only four non-zero overlapping integrals as shown in Figure II.3.1 because of spherical orientation of these atomic orbitals. The remaining cases like those shown in Figure II.3.2 correspond to the matrix elements which vanish because of symmetry constraints. σ and π bondings are defined such that the axes of the involved p orbitals are parallel and normal to the interatomic vector, respectively.

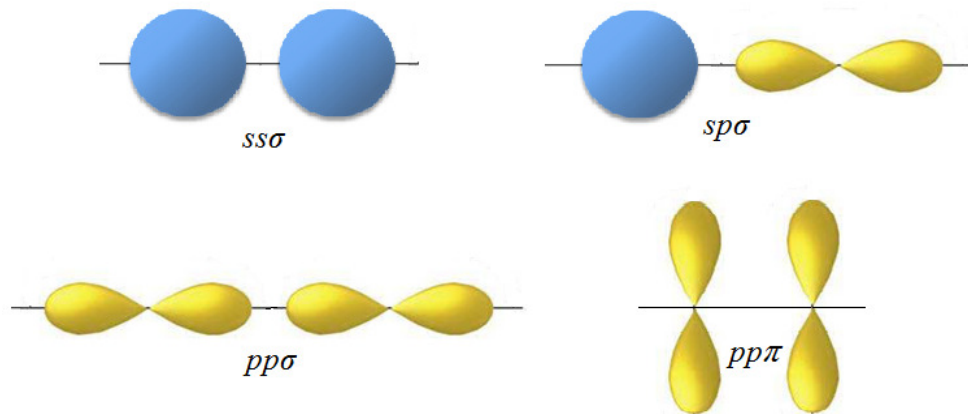


Figure II.3.1. sp -bonding correspond to non-vanishing matrix elements.

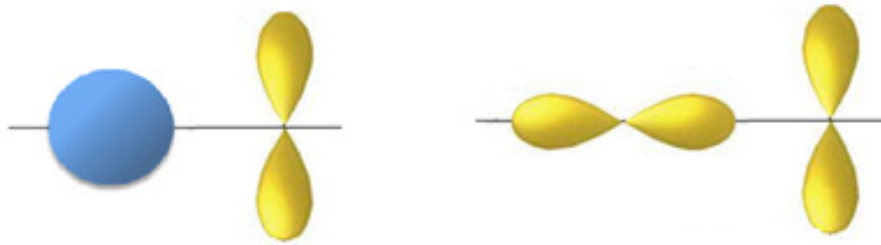


Figure II.3.2. sp -bonding correspond to vanishing matrix elements.

In general the p orbitals are not just parallel or lie on the line that joins the atomic positions. We can always project each p orbital into two components, one of them along the bonding line, the other one perpendicular to it. These are called σ and π components, respectively. This then leads to the general description of the interaction between two orbitals, or one s and one p orbital [11]. Consider the Hamiltonian matrix element between the s orbital on one atom and one of the p orbitals, which is here denoted by $|p_a\rangle$, on another atom in random directions θ relative to the joining line of their centers. Let \mathbf{d} be the unit vector along the bond and \mathbf{a} is the unit vector along one of the Cartesian axes (x, y, z) as shown in Figure II.3.3.

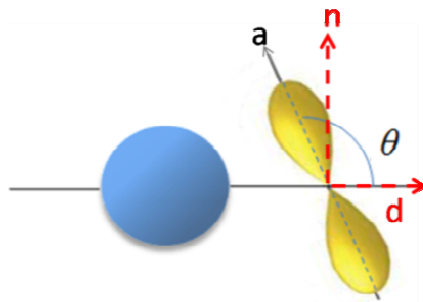


Figure II.3.3. The p orbital is in random directions θ relative to the joining line to the s orbital.

The p orbitals can be decomposed into two components that are parallel and normal to \mathbf{d} as illustrated below

$$|p_a\rangle = \mathbf{a} \cdot \mathbf{d} |p_d\rangle + \mathbf{a} \cdot \mathbf{n} |p_n\rangle = \cos \theta |p_d\rangle + \sin \theta |p_n\rangle. \quad (34)$$

Now the Hamiltonian matrix element $|s\rangle$ and $|p_a\rangle$ is given by

$$\langle s | \mathbb{H} | p_a \rangle = \langle s | \mathbb{H} | p_d \rangle \cos \theta + \langle s | \mathbb{H} | p_n \rangle \sin \theta = H_{sp\sigma} \cos \theta. \quad (35)$$

Note that the overlap between $|s\rangle$ and $|p_n\rangle$ orbitals is zero by symmetry.

Consider the Hamiltonian matrix element between $|p_1\rangle$ and $|p_2\rangle$ orbitals bonded along the unit vector \mathbf{d} in random directions θ_1 and θ_2 , respectively. This situation is shown in Figure II.3.4.

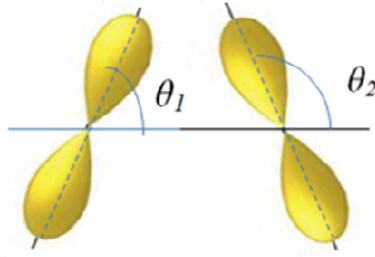


Figure II.3.4. Two p orbitals bonding in random directions.

The p orbitals can be decomposed into two components that are parallel and normal to \mathbf{d} as we have done below in (36) and demonstrated in Figure II.3.5.

$$\begin{aligned} |p_1\rangle &= \mathbf{a}_1 \cdot \mathbf{d} |p_{d1}\rangle + \mathbf{a}_1 \cdot \mathbf{n} |p_{n1}\rangle = \cos \theta_1 |p_{d1}\rangle + \sin \theta_1 |p_{n1}\rangle, \\ |p_2\rangle &= \mathbf{a}_2 \cdot \mathbf{d} |p_{d2}\rangle + \mathbf{a}_2 \cdot \mathbf{n} |p_{n2}\rangle = \cos \theta_2 |p_{d2}\rangle + \sin \theta_2 |p_{n2}\rangle. \end{aligned} \quad (36)$$

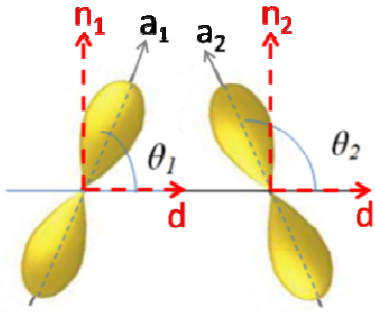


Figure II.3.5. Decomposition of p orbitals into parallel and normal components with respect to \mathbf{d} .

The Hamiltonian matrix element is then given by

$$\begin{aligned} \langle p_1 | \mathbb{H} | p_2 \rangle &= \langle p_{d1} | \mathbb{H} | p_{d2} \rangle \cos \theta_1 \cos \theta_2 + \langle p_{n1} | \mathbb{H} | p_{n2} \rangle \sin \theta_1 \sin \theta_2 \\ &= H_{pp\sigma} \cos \theta_1 \cos \theta_2 + H_{pp\pi} \sin \theta_1 \sin \theta_2, \end{aligned} \quad (37)$$

where we have used the fact that overlap between orthogonal p orbitals are zero by symmetry.

III. ENERGY BAND CALCULATION OF GRAPHENE

III.1. Introduction

Graphene is an allotrope of carbon. Its structure is one-atom-thick planar sheets of sp^2 bonded carbon atoms that are densely packed in a honeycomb crystal lattice. The honeycomb lattice can be described in terms of two triangular sub-lattices, A and B (Figure III.1.1) so there are two atoms in each unit cell.

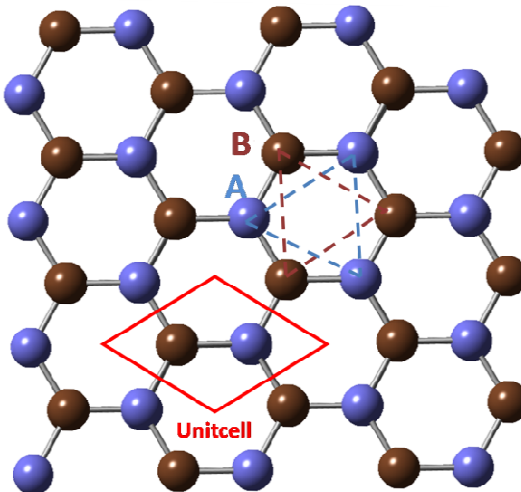


Figure III.1.1. Graphene lattice is composed of two triangular sub-lattices. The lattice constant is a .

The carbon-carbon bond length in graphene is about 1.42\AA and its lattice constant a is about 3.49\AA . The unit vectors of the underlying triangular sub-lattices are given by

$$\begin{aligned}\mathbf{a}_1 &= \frac{a}{2}(\sqrt{3}, +1), \\ \mathbf{a}_2 &= \frac{a}{2}(\sqrt{3}, -1).\end{aligned}\quad (38)$$

Graphene is a new material, and known to be not only the thinnest ever semimetal, but also the strongest material, too. As a conductor of electricity, it performs as well as copper. As a conductor of heat it outperforms all other known materials. It is almost completely transparent, yet so dense that not even helium, the smallest atomic gas, can pass through it. Furthermore, graphene is an excellent support of spin-current, and provides an ideal support bed for the future spintronic devices [12].

Graphene is a basic building block for graphitic materials of all other dimensionalities. It can be wrapped up into 0D fullerenes, rolled into 1D nanotubes or stacked into 3D graphite [13]. Graphite is obtained by stacking of graphene layers that is stabilized by weak van der Waals interactions [14]. Diamond also can be obtained from graphene under extreme pressure and temperatures. Carbon nanotubes are formed by graphene wrapping, while

fullerenes are obtainable from graphene by modifying the hexagons into pentagons and heptagons in a systematic way [15]. It is obvious that there has been enormous interest in understanding physical properties of graphene. Graphene has been the subject of many recent investigations due to its peculiar transport properties [16, 17]. The 2010 Nobel Prize in Physics has been awarded to Andre Geim and Konstantin Novoselov for groundbreaking experiments regarding the two-dimensional material graphene [18] (Figure III.1.3).

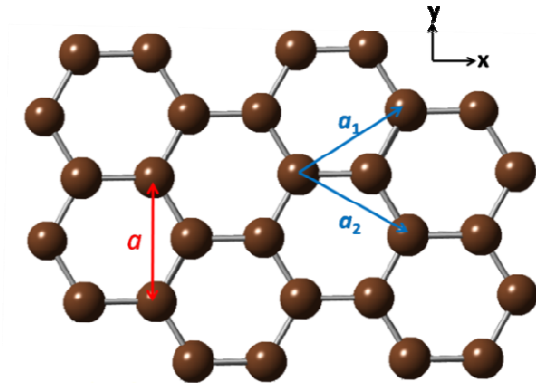


Figure III.1.2. The unit vectors and unit cell in graphene lattice.



Figure III.1.3. Konstantin Novoselov (on the left) accepts the Nobel Prize in Physics in December 10, 2010, “for groundbreaking experiments regarding the two-dimensional material graphene” [18].

III.2. Orbital Hybridization in Graphene

Graphene is a flat monolayer of carbon atoms tightly packed into a two-dimensional (2D) honeycomb lattice. Because of this, carbon atoms have the sp^2 hybridization. In this case, three

σ bonds lie on the same plane with bond angles 120° . The remaining $2p_z$ orbital for each carbon overlaps to form a π bond.

III.3. Calculation of σ Bands Using TB

The σ bands are related to σ bonds between carbon atoms. It is should be pointed out that each unit cell of graphene has two carbon atoms with sp^2 hybridization, and every atom participates with three $2s$, $2p_x$ and $2p_y$ orbitals in the bonding. Thus we deal with six orbitals in each unit cell yielding six σ bands, three of which appear below the Fermi energy called σ , and the other three above the Fermi energy being referred to as σ^* .

We have to use the secular equation (14). Here the transfer and overlap matrices are represented by 6×6 matrices.

We start with the transfer matrix

$$\begin{aligned}
 H = & \begin{array}{c|ccccc}
 2s_A & 2p_{xA} & 2p_{yA} & 2s_B & 2p_{xB} & 2p_{yB} \\
 \hline
 2s_A & H_{11} & \dots & \dots & \dots & H_{16} \\
 2p_{xA} & \vdots & \ddots & & & \vdots \\
 2p_{yA} & \vdots & & \ddots & & \vdots \\
 \hline
 2s_B & & & \ddots & & \vdots \\
 2p_{xB} & \vdots & & & \ddots & \vdots \\
 2p_{yB} & H_{61} & \dots & \dots & \dots & H_{66}
 \end{array}_{6 \times 6} \\
 & = \begin{bmatrix} H_{AA} & H_{AB} \\ H_{BA} & H_{BB} \end{bmatrix}. \tag{39}
 \end{aligned}$$

Here, AA and AB terms belong to integrals between orbitals of atom A in the unit cell, and between A and B atomic orbitals, respectively.

Written out in component form, the H_{AA} is

$$\begin{aligned}
 H_{AA}(\mathbf{k}) &= \langle \phi_A | \mathbb{H} | \phi_A \rangle \\
 &= \frac{1}{N} \sum_{\mathbf{R}_A}^N \sum_{\mathbf{R}'_A} e^{i\mathbf{k} \cdot (\mathbf{R}_A - \mathbf{R}'_A)} \langle \varphi(\mathbf{r} - \mathbf{R}_A) | \mathbb{H} | \varphi(\mathbf{r} - \mathbf{R}'_A) \rangle \\
 &= \frac{1}{N} \sum_{\substack{\mathbf{R}_A = \mathbf{R}'_A}}^N \langle \varphi(\mathbf{r} - \mathbf{R}_A) | \mathbb{H} | \varphi(\mathbf{r} - \mathbf{R}_A) \rangle.
 \end{aligned} \tag{40}$$

Each matrix element is determined using below relations

$$\begin{aligned}
h_{11} &= \left\langle \phi_{2s} \left| \mathbb{H} \right| \phi_{2s} \right\rangle = \frac{1}{N} \sum_{\mathbf{R}_A = \mathbf{R}'_A}^N \left\langle \varphi_{2s}(\mathbf{r} - \mathbf{R}_A) \left| \mathbb{H} \right| \varphi_{2s}(\mathbf{r} - \mathbf{R}_A) \right\rangle = \varepsilon_{2s}, \\
h_{22} &= \left\langle \phi_{2p_x} \left| \mathbb{H} \right| \phi_{2p_x} \right\rangle = \frac{1}{N} \sum_{\mathbf{R}_A = \mathbf{R}'_A}^N \left\langle \varphi_{2p_x}(\mathbf{r} - \mathbf{R}_A) \left| \mathbb{H} \right| \varphi_{2p_x}(\mathbf{r} - \mathbf{R}_A) \right\rangle = \varepsilon_{2p}, \quad (41) \\
h_{33} &= \left\langle \phi_{2p_y} \left| \mathbb{H} \right| \phi_{2p_y} \right\rangle = h_{22} = \varepsilon_{2p}.
\end{aligned}$$

The remaining terms are zero because of the spherical harmonics $Y_{lm}(\theta, \varphi)$ of p_x and p_y orbitals. In the tabular form, H_{AA} is given by

$$H_{AA} = \begin{pmatrix} \varepsilon_{2s} & 0 & 0 \\ 0 & \varepsilon_{2p} & 0 \\ 0 & 0 & \varepsilon_{2p} \end{pmatrix}. \quad (42)$$

Suggested model parameters values fitted to the electronic band structure along the high-symmetry lines are $\varepsilon_{2s} = -8.7$ eV and $\varepsilon_{2p} = 0$ eV.

We define tabular form of H_{AB} as

$$H_{AB} = \begin{pmatrix} h_{11} & h_{12} & h_{13} \\ h_{21} & h_{22} & h_{23} \\ h_{31} & h_{32} & h_{33} \end{pmatrix} \quad (43)$$

which its components have the general form

$$H_{AB}(\mathbf{k}) = \left\langle \phi_A \left| \mathbb{H} \right| \phi_B \right\rangle = \frac{1}{N} \sum_{\mathbf{R}_A}^N \sum_{\mathbf{R}_B}^N e^{i\mathbf{k} \cdot (\mathbf{R}_A - \mathbf{R}_B)} \left\langle \varphi(\mathbf{r} - \mathbf{R}_A) \left| \mathbb{H} \right| \varphi(\mathbf{r} - \mathbf{R}_B) \right\rangle. \quad (44)$$

Here we consider only the nearest-neighbor interaction. There are three such nearest neighbors, and hence the vectors \mathbf{R}_{Ai} are given by

$$\begin{aligned}
\mathbf{R}_{A1} &= \frac{a}{\sqrt{3}}(-1, 0), \\
\mathbf{R}_{A2} &= \frac{a}{2\sqrt{3}}(1, +\sqrt{3}), \\
\mathbf{R}_{A3} &= \frac{a}{2\sqrt{3}}(1, -\sqrt{3}).
\end{aligned} \quad (45)$$

As discussed before, a is the lattice constant of the graphene. Figure III.3.1 shows these vectors.

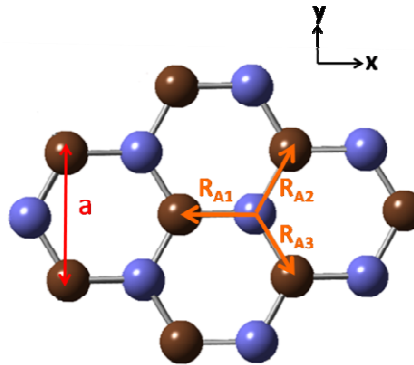


Figure III.3.1. Three nearest neighbors of the carbon atom shown by \mathbf{R}_{Ai} vectors.

Because of the different orientations of the nearest-neighbor atoms B_i correspond to the atom A , it is necessary to consider general forms for (40) and (42). Hence, one can write H_{AB} components as

$$\begin{aligned} h_{11} &= \langle \phi_{A2s} | \mathbb{H} | \phi_{B2s} \rangle = \frac{1}{N} \sum_{\mathbf{R}_A} \sum_{\mathbf{R}_B} e^{i\mathbf{k} \cdot (\mathbf{R}_A - \mathbf{R}_B)} \langle \varphi_{A2s}(\mathbf{r} - \mathbf{R}_A) | \mathbb{H} | \varphi_{B2s}(\mathbf{r} - \mathbf{R}_B) \rangle \\ &= H_{ss\sigma} \sum_{i=1}^3 e^{i\mathbf{k} \cdot \mathbf{R}_{Ai}}. \end{aligned} \quad (46)$$

\mathbf{R}_{Ai} are the vectors pointing from A to B_i atoms. As it was discussed above, these vectors show the nearest neighbors of A atom. Therefore, we get the following

$$\begin{aligned} h_{12} &= \langle \phi_{A2s} | \mathbb{H} | \phi_{B2p_x} \rangle \\ &= \frac{1}{N} \sum_{\mathbf{R}_A} \sum_{\mathbf{R}_B} e^{i\mathbf{k} \cdot (\mathbf{R}_A - \mathbf{R}_B)} \langle \varphi_{A2s}(\mathbf{r} - \mathbf{R}_A) | \mathbb{H} | \varphi_{B2p_x}(\mathbf{r} - \mathbf{R}_B) \rangle \\ &= H_{sp\sigma} \sum_{i=1}^3 e^{i\mathbf{k} \cdot \mathbf{R}_{Ai}} \cos \theta, \end{aligned} \quad (47)$$

$$\begin{aligned} h_{13} &= \langle \phi_{A2s} | \mathbb{H} | \phi_{B2p_y} \rangle \\ &= \frac{1}{N} \sum_{\mathbf{R}_A} \sum_{\mathbf{R}_B} e^{i\mathbf{k} \cdot (\mathbf{R}_A - \mathbf{R}_B)} \langle \varphi_{A2s}(\mathbf{r} - \mathbf{R}_A) | \mathbb{H} | \varphi_{B2p_y}(\mathbf{r} - \mathbf{R}_B) \rangle \\ &= H_{sp\sigma} \sum_{i=1}^3 e^{i\mathbf{k} \cdot \mathbf{R}_{Ai}} \sin \theta, \end{aligned} \quad (48)$$

$$\begin{aligned}
h_{22} &= \left\langle \phi_{A2p_x} \left| \mathbb{H} \right| \phi_{B2p_x} \right\rangle \\
&= \frac{1}{N} \sum_{\mathbf{R}_A}^N \sum_{\mathbf{R}_B} e^{i\mathbf{k} \cdot (\mathbf{R}_A - \mathbf{R}_B)} \left\langle \varphi_{A2p_x}(\mathbf{r} - \mathbf{R}_A) \left| \mathbb{H} \right| \varphi_{B2p_x}(\mathbf{r} - \mathbf{R}_B) \right\rangle \quad (49) \\
&= \sum_{i=1}^3 \left[H_{pp\sigma} \cos^2 \theta + H_{pp\pi} (1 - \cos^2 \theta) \right] e^{i\mathbf{k} \cdot \mathbf{R}_{Ai}},
\end{aligned}$$

$$\begin{aligned}
h_{23} &= \left\langle \phi_{A2p_x} \left| \mathbb{H} \right| \phi_{B2p_y} \right\rangle \\
&= \frac{1}{N} \sum_{\mathbf{R}_A}^N \sum_{\mathbf{R}_B} e^{i\mathbf{k} \cdot (\mathbf{R}_A - \mathbf{R}_B)} \left\langle \varphi_{A2p_x}(\mathbf{r} - \mathbf{R}_A) \left| \mathbb{H} \right| \varphi_{B2p_y}(\mathbf{r} - \mathbf{R}_B) \right\rangle \quad (50) \\
&= \sum_{i=1}^3 (H_{pp\sigma} - H_{pp\pi}) \cos \theta \sin \theta e^{i\mathbf{k} \cdot \mathbf{R}_{Ai}},
\end{aligned}$$

$$\begin{aligned}
h_{33} &= \left\langle \phi_{A2p_y} \left| \mathbb{H} \right| \phi_{B2p_y} \right\rangle \\
&= \frac{1}{N} \sum_{\mathbf{R}_A}^N \sum_{\mathbf{R}_B} e^{i\mathbf{k} \cdot (\mathbf{R}_A - \mathbf{R}_B)} \left\langle \varphi_{A2p_y}(\mathbf{r} - \mathbf{R}_A) \left| \mathbb{H} \right| \varphi_{B2p_y}(\mathbf{r} - \mathbf{R}_B) \right\rangle \quad (51) \\
&= \sum_{i=1}^3 \left[H_{pp\sigma} \sin^2 \theta + H_{pp\pi} (1 - \sin^2 \theta) \right] e^{i\mathbf{k} \cdot \mathbf{R}_{Ai}}.
\end{aligned}$$

Other parameters can be written based on the facts that $\langle s | \mathbb{H} | p \rangle = -\langle p | \mathbb{H} | s \rangle$, $\langle p_1 | \mathbb{H} | p_2 \rangle = \langle p_2 | \mathbb{H} | p_1 \rangle$ and $\langle s_1 | \mathbb{H} | s_2 \rangle = \langle s_2 | \mathbb{H} | s_1 \rangle$. We choose the model parameters value to be $H_{sp\sigma} = 5.5$ eV, $H_{ss\sigma} = -6.7$ eV, $H_{pp\sigma} = 5.1$ eV, and $H_{pp\pi} = -3.1$ eV, which are close to reported values in [8]. These parameters are obtained from a fit to the experimental electronic band structure along the high-symmetry lines.

The same treatment yields the overlap matrix elements. We assume that the atomic wavefunctions are normalized as shown in (17), so the S_{AA} matrix is given by

$$S_{AA} = \begin{pmatrix} 1 & 0 & 0 \\ 0 & 1 & 0 \\ 0 & 0 & 1 \end{pmatrix}. \quad (52)$$

Similarly to H_{AB} , the elements of S_{AB} is described as below

$$s_{11} = \left\langle \phi_{A2s} \left| \phi_{B2s} \right. \right\rangle = S_{ss\sigma} \sum_{i=1}^3 e^{i\mathbf{k} \cdot \mathbf{R}_{Ai}}, \quad (53)$$

$$s_{12} = \left\langle \phi_{A2s} \left| \phi_{B2p_x} \right. \right\rangle = S_{sp\sigma} \sum_{i=1}^3 e^{i\mathbf{k} \cdot \mathbf{R}_{Ai}} \cos \theta, \quad (54)$$

$$s_{13} = \left\langle \phi_{A2s} \left| \phi_{B2p_y} \right. \right\rangle = S_{sp\sigma} \sum_{i=1}^3 e^{i\mathbf{k} \cdot \mathbf{R}_{Ai}} \sin \theta, \quad (55)$$

$$s_{22} = \left\langle \phi_{A2p_x} \middle| \phi_{B2p_x} \right\rangle = \sum_{i=1}^3 [S_{pp\sigma} \cos^2 \theta + S_{pp\pi} (1 - \cos^2 \theta)] e^{i\mathbf{k} \cdot \mathbf{R}_{Ai}}, \quad (56)$$

$$s_{23} = \left\langle \phi_{A2p_x} \middle| \phi_{B2p_y} \right\rangle = \sum_{i=1}^3 e^{i\mathbf{k} \cdot \mathbf{R}_{Ai}} (S_{pp\sigma} - S_{pp\pi}) \cos \theta \sin \theta, \quad (57)$$

$$s_{33} = \left\langle \phi_{A2p_y} \middle| \phi_{B2p_y} \right\rangle = \sum_{i=1}^3 [S_{pp\sigma} \sin^2 \theta + S_{pp\pi} (1 - \sin^2 \theta)] e^{i\mathbf{k} \cdot \mathbf{R}_{Ai}}. \quad (58)$$

Other parameters can be written based on the facts that $\langle s | p \rangle = -\langle p | s \rangle$, $\langle p_1 | p_2 \rangle = \langle p_2 | p_1 \rangle$, and $\langle s_1 | s_2 \rangle = \langle s_2 | s_1 \rangle$. Suggested tight-binding parameters are $S_{sp\sigma} = -0.10 \text{ eV}$, $S_{ss\sigma} = 0.20 \text{ eV}$, $S_{pp\sigma} = -0.15 \text{ eV}$, and $S_{pp\pi} = 0.12 \text{ eV}$.

The two carbon atoms in the unit cell of graphene are identical. Hence the transfer matrix element H_{AA} , which is given by the interaction of an atom at site A with itself and all other A atoms in the crystal, is exactly the same as H_{BB} . Similarly, H_{AB} is simply the complex conjugate of H_{BA} . This condition is also satisfied for S_{AA} and S_{BB} , and S_{AB} and S_{BA} . So we have

$$\begin{aligned} H_{BB} &= H_{AA}, & H_{BA} &= H_{AB}^*, \\ S_{BB} &= S_{AA}, & S_{BA} &= S_{AB}^*. \end{aligned} \quad (59)$$

Finally, the secular equation is expressed in the most general form of

$$\begin{bmatrix} H_{AA(3 \times 3)} & H_{AB(3 \times 3)} \\ H_{BA(3 \times 3)} & H_{BB(3 \times 3)} \end{bmatrix} - E(\mathbf{k}) \begin{bmatrix} S_{AA(3 \times 3)} & S_{AB(3 \times 3)} \\ S_{BA(3 \times 3)} & S_{BB(3 \times 3)} \end{bmatrix} = 0. \quad (60)$$

Solving this eigenvalue problem yields the electronic band structure of graphene. Since all possible eigenstates are specified by the wavevector \mathbf{k} within any one primitive cell of the periodic lattice in reciprocal space, the first Brillouin zone is the uniquely defined cell that is the most compact possible cell. So it is enough to calculate the band structure in this region. For graphene, the first Brillouin zone is a hexagon. In this case, six symmetry axes exist which can be deduced from one another by rotations of $\pi/6$ with an invariance under rotation equal to $\pi/3$. Figure III.3.2 shows this region.

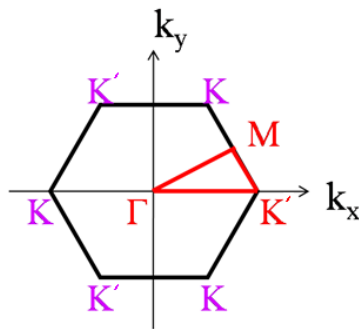


Figure III.3.2. First Brillouin zone of the hexagonal lattice. The irreducible zone is shown in red.

The range over which \mathbf{k} is studied can be further reduced by considering the other symmetries which constitutes the irreducible Brillouin zone of the hexagonal lattice. It can be demonstrated that the irreducible Brillouin zone is the half of an equilateral triangle with apexes Γ , K and M as shown in Figure III.3.2. It is generally sufficient to let the wave vector \mathbf{k} describes the edge of the irreducible Brillouin zone, while the inner region is ignored.

Figure III.3.3 shows the σ band structure of the graphene lattice calculated using Tight-binding model [19].

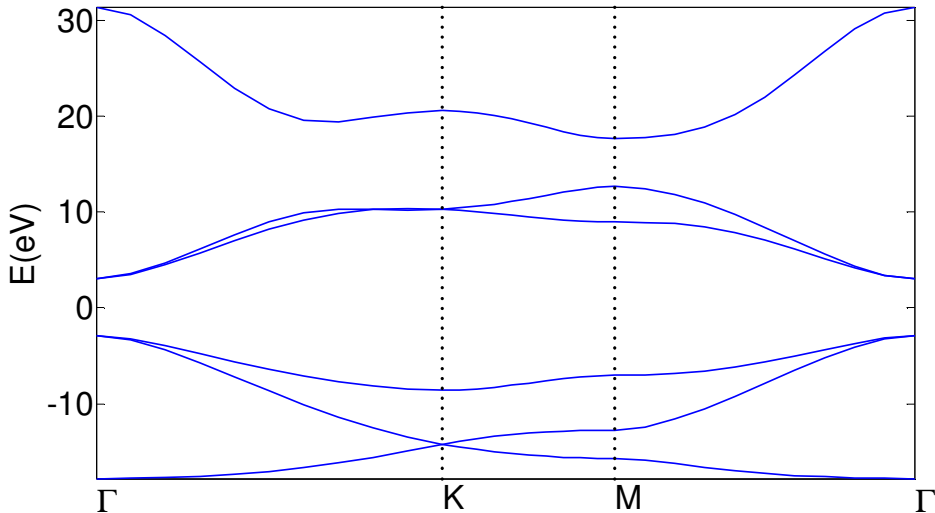


Figure III.3.3. σ electronic band structure of graphene calculated using tight-binding method.

III.4. Calculation of π Bands Using TB

Band structure of graphene around the Fermi level and for transition energies well above the optical range is determined by π orbitals; the Fermi level is normally placed at the Dirac point for unbiased and undoped graphene. A common approximation for the low energy electronic properties is hence a tight-binding Hamiltonian including only the carbon $2p_z$ states. These orbitals are all parallel to one another and each contains one electron (Figure III.4.1).

As mentioned before, each unit cell of graphene has two carbon atoms which construct π bonds using p_z orbitals. Using the secular equation (14), the transfer and overlap matrices are obtained as 2×2 matrices.

We start with transfer matrix

$$[H] = \begin{array}{c} 2p_{zA} & 2p_{zB} \\ \hline \hline 2p_{zA} & \left(\begin{array}{c|c} H_{AA} & H_{AB} \\ \hline H_{BA} & H_{BB} \end{array} \right)_{2 \times 2} \\ 2p_{zB} & \end{array} . \quad (61)$$

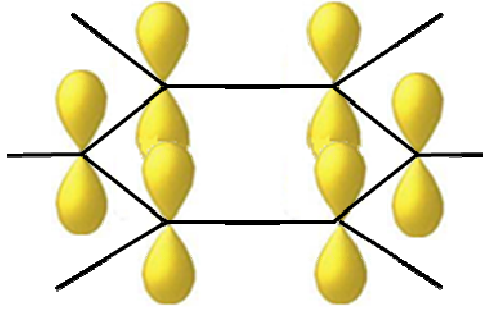


Figure III.4.1. p orbitals of carbon atoms in the graphene structure.

Written out in component form, the $[H]$ is

$$\begin{aligned} H_{AA} &= \langle \phi_{2p_z} | H | \phi_{2p_z} \rangle \\ &= \frac{1}{N} \sum_{\mathbf{R}_A=\mathbf{R}'_A}^N \langle \varphi_{2p_z}(\mathbf{r} - \mathbf{R}_A) | H | \varphi_{2p_z}(\mathbf{r} - \mathbf{R}_A) \rangle = \varepsilon_{2p}, \end{aligned} \quad (62)$$

$$\begin{aligned} H_{AB} &= \langle \phi_{A2p_z} | H | \phi_{B2p_z} \rangle \\ &= \frac{1}{N} \sum_{\mathbf{R}_A}^N \sum_{\mathbf{R}_B}^N e^{i\mathbf{k} \cdot (\mathbf{R}_A - \mathbf{R}_B)} \langle \varphi_{A2p_z}(\mathbf{r} - \mathbf{R}_A) | H | \varphi_{B2p_z}(\mathbf{r} - \mathbf{R}_B) \rangle \\ &= \sum_{i=1}^3 H_{pp\pi} e^{i\mathbf{k} \cdot \mathbf{R}_{Ai}}. \end{aligned} \quad (63)$$

The same treatment yields the overlap matrix elements as follows

$$[S] = \begin{array}{c} 2p_{zA} & 2p_{zB} \\ \hline \hline 2p_{zA} & \left(\begin{array}{c|c} S_{AA} & S_{AB} \\ \hline S_{BA} & S_{BB} \end{array} \right)_{2 \times 2} \\ 2p_{zB} & \end{array} \quad (64)$$

which can be written out in the component form

$$S_{AA} = \langle \phi_{2p_z} | \phi_{2p_z} \rangle = \frac{1}{N} \sum_{\mathbf{R}_A=\mathbf{R}'_A}^N \langle \varphi_{2p_z}(\mathbf{r} - \mathbf{R}_A) | \varphi_{2p_z}(\mathbf{r} - \mathbf{R}_A) \rangle = 1, \quad (65)$$

$$\begin{aligned}
S_{AB} &= \left\langle \phi_{A2p_z} \mid \phi_{B2p_z} \right\rangle = \\
&= \frac{1}{N} \sum_{\mathbf{R}_A}^N \sum_{\mathbf{R}_B} e^{i\mathbf{k}\cdot(\mathbf{R}_A - \mathbf{R}_B)} \left\langle \varphi_{A2p_z}(\mathbf{r} - \mathbf{R}_A) \mid \varphi_{B2p_z}(\mathbf{r} - \mathbf{R}_B) \right\rangle \\
&= \sum_{i=1}^3 S_{pp\pi} e^{i\mathbf{k}\cdot\mathbf{R}_{Ai}}.
\end{aligned} \quad (66)$$

Again, in (65) we assume that the atomic wave functions are normalized.

As mentioned before, the transfer matrix element H_{AA} , given by the interaction of an atom at site A with itself and all other A atoms in the crystal, is exactly the same as H_{BB} . Similarly, H_{AB} is simply the complex conjugate of H_{BA} . This condition is also satisfied for S_{AA} , S_{BB} , and S_{AB} and S_{BA} .

The secular equation is constructed as below

$$\begin{vmatrix} H_{AA(1\times 1)} & H_{AB(1\times 1)} \\ H_{BA(1\times 1)} & H_{BB(1\times 1)} \end{vmatrix} - E(\mathbf{k}) \begin{vmatrix} S_{AA(1\times 1)} & S_{AB(1\times 1)} \\ S_{BA(1\times 1)} & S_{BB(1\times 1)} \end{vmatrix} = 0. \quad (67)$$

Solving this eigenvalue problem yields to the π electronic bands of graphene shown in Figure III.4.2 [19].

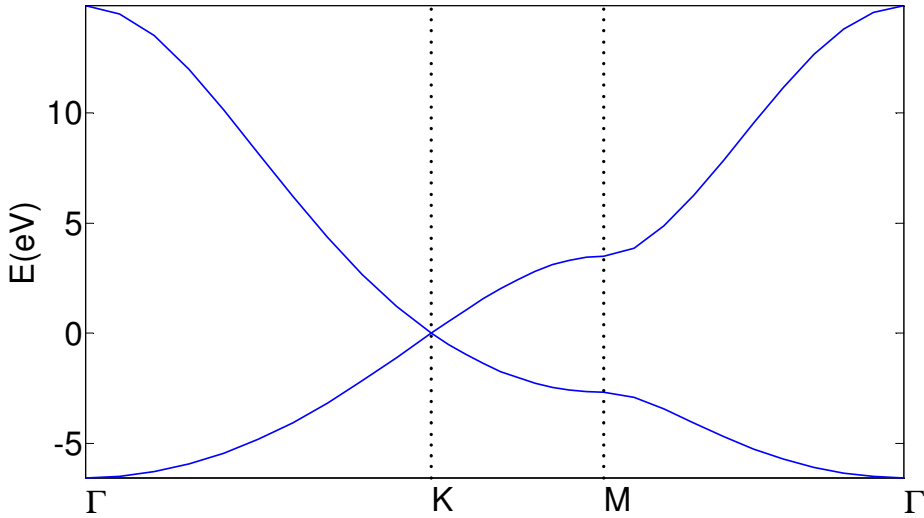


Figure III.4.2. π electronic band structure calculated using tight-binding method.

Figure III.4.3 shows σ and π band structures of graphene together. There is a very good agreement between these results and those reported in [20] obtained from first-principles calculations shown in Figure III.4.4.

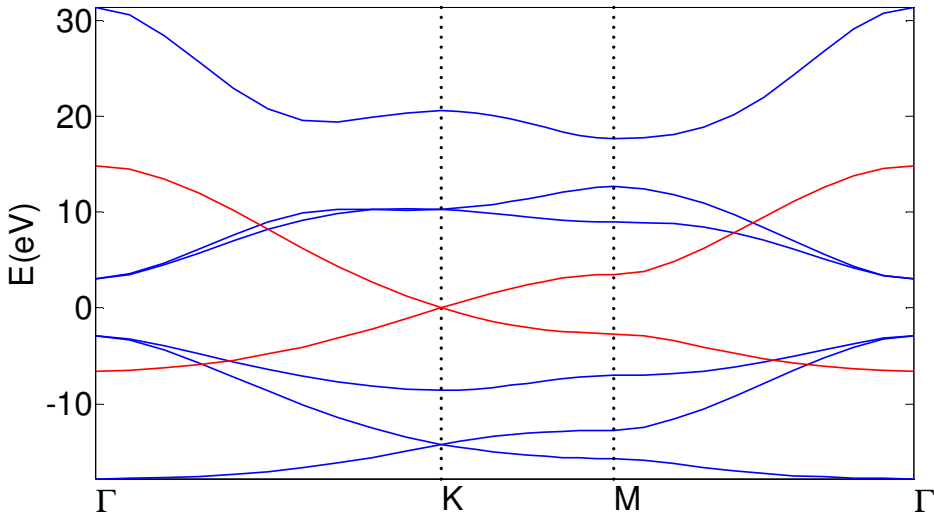


Figure III.4.3. σ (blue) and π (red) band structures calculated using Tight-binding method.

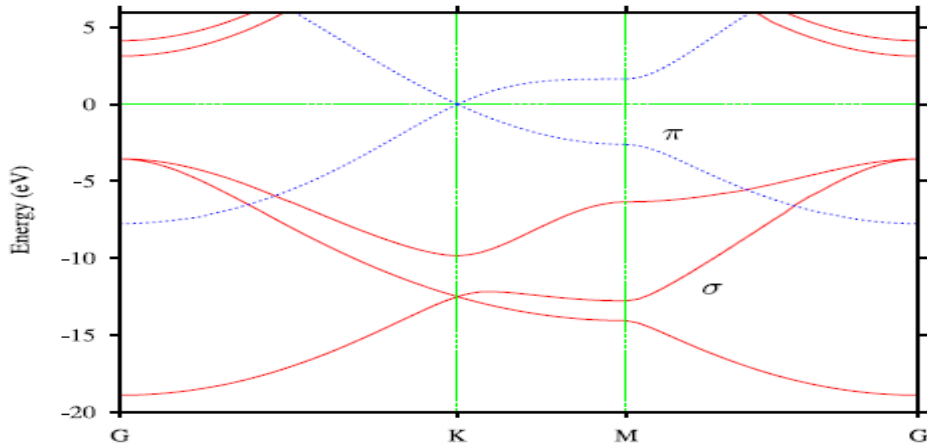


Figure III.4.4. σ (red) and π (dashed blue) band structures from first-principles calculations [20].

It is remarkable that graphene is a gapless semiconductor, with no gap at the Dirac point [16]. Many interesting ways have been proposed and investigated to tune the band gap of graphene. However, it is well known that the presence of defects such as vacancies or impurities [19, 21, 22], the interaction with a substrate [23], or the edge structure in graphene nanoribbons [24, 25, 26] can lead to a bandgap opening in graphene.

The idea of introducing a periodic array of vacancies into the graphene lattice was first mentioned in [19]. Many works have been done with the same idea, since then, on the so-called anti-dot graphene lattices [27, 28, 29, 30, 31].

Electronic structures of coupled semiconductor quantum dots arranged as graphene hexagonal lattice are studied theoretically using the tight-binding method up to the third-nearest-

neighbors. The novel two-dimensional Dirac-like electronic excitations in graphene are found in these artificial planar quantum dot structures which provide the theoretical basis for searching Dirac fermions in quantum dot materials and have great significance for investigating and making semiconductor quantum dot devices [32].

Band gap engineering in hexagonal h-BN antidot lattices is another work done in this field. Although graphene is a gapless semimetal due to the symmetry between two sublattices of the honeycomb structure, h-BN is a semiconductor with a wide bandgap around 5.5 eV [33]. It is found that when the anti-dot lattice is along the zigzag direction, the band gap opening can be related to the intervalley scattering and does not follow the simple scaling rule previously proposed in the literature for the anti-dot lattice along the armchair direction. For h-BN, the calculations show that the anti-dot lattice results in reducing of band gaps. Coupled with doping of carbon atoms, the bandgap of h-BN antidot lattice can be reduced to below 2 eV, which might have implications in light-emitting devices or photo-electrochemistry [34].

Regular hydrogen adsorption on graphene is another way to open a bandgap in graphene [35] to be discussed briefly later in the next section.

IV. ENERGY BAND CALCULATION OF GRAPHANE

IV.1. Introduction

The chemical modification of graphene to create derivatives with different structures and properties has so far been restricted to graphene oxide [36, 37, 38], a disordered structure that bears an assortment of functional groups.

Another possible modification, which has been predicted theoretically [39], is the addition of hydrogen atoms to graphene, altering the sp^2 hybridization of carbon atoms to sp^3 , and thus changing the structure and electronic properties, to form a new two-dimensional hydrocarbon called graphane. Recently, the Nobel Laureates Andre Geim and Konstantin Novoselov from the University of Manchester and co-workers from Russia and the Netherlands have hydrogenated mechanically exfoliated graphene by exposing it to hydrogen plasma [40]. The electronic properties of the new material change markedly: the highly conductive graphene is converted from a semimetal into a semiconductor. Because of its structure and lowdimensionality, it provides a fertile playground for fundamental science andtechnological applications.

It is reported that hydrogenation of mono, bi, and trilayer graphene samples via exposure to H₂ plasma occurs as a result of electron irradiation of H₂O adsorbates on the samples, rather than H species in the plasma as reported [41]. It is proposed that the hydrogenation mechanism is electron-impact fragmentation of H₂O adsorbates into H⁺ ions. At the incident electron energies of 60eV, hydrogenation is observed which is significantly more stable at temperatures 200°C than previously reported [42].

This hexagonal arrangement of carbons in the sp^3 hybridization with C: H = 1 forms two constructions: if the H atoms connect at opposite sides of the plane of C-C bond, it is called *chairlike*, as illustrated in Figure IV.1.1, and if on the same side of the C-C plane, it is called *boatlike*. The typical C-C bond length for chair like conformer is 1.52Å which is similar to the sp^3 bond length of 1.53Å in diamond and that for boatlike conformer it is 1.56Å [39].

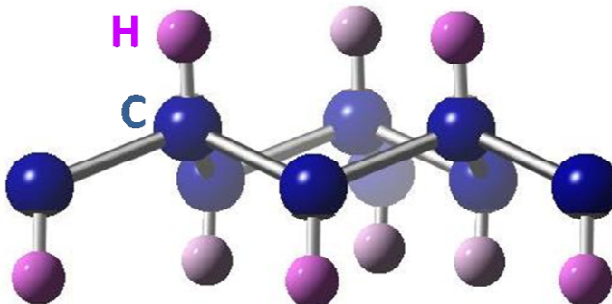


Figure IV.1.1. The chairlike structure of graphane.

Graphane was first predicted to exist only in the boat and chair configurations [37]. But a new report has just pointed out that the existence of a new conformer, being referred to as the stirrup, is also plausible [42]. Nevertheless, all these three conformers are expected to exhibit very close chemical and physical properties. The structural and phonon properties of these structures, as well as their relative stability can be established by first-principles calculations. It is shown that all these three graphane conformers respond to any arbitrarily oriented extension with a much smaller lateral contraction than the one calculated for graphene. Furthermore, the boatlike-graphane has a small and negative Poisson ratio along the armchair and zigzag principal directions of the carbon honeycomb lattice. Moreover, the chairlike-graphane admits both softening and hardening hyperelasticity, depending on the direction of applied load [43]. Lattice thermal properties of graphane lattice have been also calculated [44]. Some further properties of graphene/graphane interfaces are discussed in [45, 46]. It is also anticipated that doped graphane could serve as a high temperature superconductor with a transition temperature well exceeding 90K [47, 48, 49].

IV.2. Orbital Hybridization in Graphene

Graphane is again an arrangement of carbon atoms with sp^3 hybridization saturated by hydrogen forming a honeycomb shape. Transformation of the sp^2 hybridization in graphene to the sp^3 hybridization in graphane results in a change of the bond lengths and angles (Figure IV.2.1).

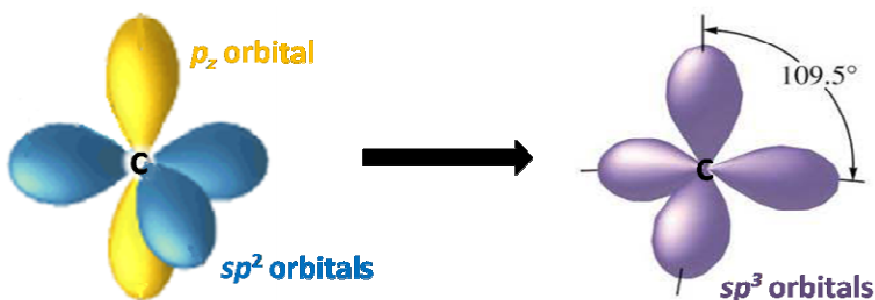


Figure IV.2.1. Transformation of the sp^2 hybridization of carbon to the sp^3 .

A typical bond length for sp^2 C-C bond and the standard bond angle for graphene and graphite is 1.42 Å and 120°, respectively. For sp^3 hybridization, the standard value of C-C bond length is 1.54 Å, and the corresponding angle is 109.5°. A typical value for the single C-H bond length is about 1.14 Å. But in graphane, depending on the number of the added hydrogen, the length of C-C bond is between 1.42 Å and 1.54 Å. Also C-C-H and C-C-C angles are intermediate between 90° and 109.5° and 120° and 109.5°, respectively. This implies an intermediate character of the hybridization between sp^2 and sp^3 [50].

IV.3. Electronic Band Structure Calculated Using TB

As mentioned before, graphane is a honeycomb structure of carbon atoms which their p_z orbitals are saturated with hydrogen atoms. Here we consider chairlike structure. The top view of this structure is a hexagonal shape, like in graphene. Thus, its unit cell has a rhombus cross section and there are four atoms in each unit cell: two carbon and two hydrogen atoms as shown in Figure IV.3.1.

Each carbon atom participates in the bonding in sp^3 hybridization using $2s$, $2p_x$, $2p_y$ and $2p_z$ orbitals. Each hydrogen atom also participates through its $1s$ orbital. Hence, the Hamiltonian matrix related to (25) and (26) is sized originally as 10×10 .

Therefore, Hamiltonian matrix has a general form given as

$$[\mathbf{H}] = \begin{array}{c|ccccc|ccccc} & 2s_A & 2p_{xA} & 2p_{yA} & 2p_{zA} & 1s_A & 2s_B & 2p_{xB} & 2p_{yB} & 2p_{zB} & 1s_B \\ \hline & H_{11} & & & & & & & & & H_{1,10} \\ & \ddots & & & & & & & & & \\ & & \ddots & & & & & & & & \\ & & & \ddots & & & & & & & \\ & & & & \ddots & & & & & & \\ & & & & & \ddots & & & & & \\ & & & & & & \ddots & & & & \\ & & & & & & & \ddots & & & \\ & & & & & & & & \ddots & & \\ & & & & & & & & & H_{10,10} & \\ \hline & 2s_A & & & & & & & & & \\ & 2p_{xA} & & & & & & & & & \\ & 2p_{yA} & & & & & & & & & \\ & 2p_{zA} & & & & & & & & & \\ & 1s_A & & & & & & & & & \\ \hline & 2s_B & & & & & & & & & \\ & 2p_{xB} & & & & & & & & & \\ & 2p_{yB} & & & & & & & & & \\ & 2p_{zB} & & & & & & & & & \\ & 1s_B & & & & & & & & & \\ \hline & & H_{10,1} & & & & & & & & \end{array}_{10 \times 10}$$

$$= \begin{pmatrix} H_{AA} & & H_{AB} \\ & \hline & \\ H_{BA} & & H_{BB} \end{pmatrix}. \quad (68)$$

A and *B* terms belong to each carbon and hydrogen connected to it in the unit cell as labeled in Figure IV.3.1.

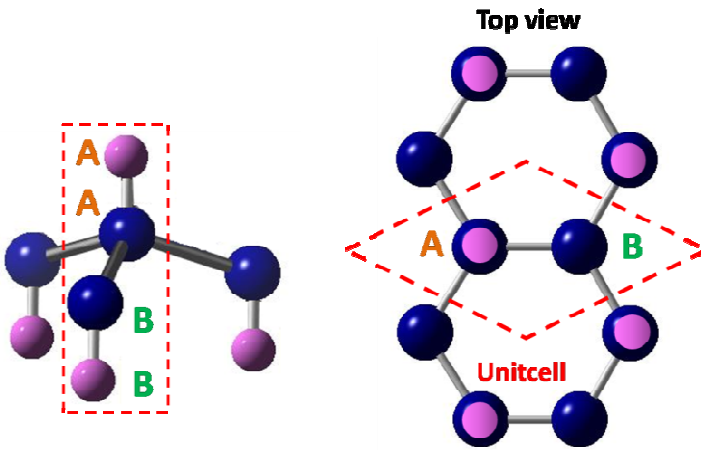


Figure IV.3.1. Unit cell of chairlike graphane.

We define tabular form of H_{AA} as

$$H_{AA} = \begin{pmatrix} h_{11} & h_{12} & h_{13} & h_{14} & h_{15} \\ h_{21} & h_{22} & h_{23} & h_{24} & h_{25} \\ h_{31} & h_{32} & h_{33} & h_{34} & h_{35} \\ h_{41} & h_{42} & h_{43} & h_{44} & h_{45} \\ h_{51} & h_{52} & h_{53} & h_{54} & h_{55} \end{pmatrix}. \quad (69)$$

This matrix is referred to on-site energies as defined in (25). Writing out H_{AA} in its components gives

$$h_{ji} = \langle \varphi_m(\mathbf{r} - \mathbf{t}_j) | \mathbb{H} | \varphi_l(\mathbf{r} - \mathbf{t}_i - \mathbf{R}) \rangle = \delta_{lm} \delta_{ij} \delta(\mathbf{R}) \varepsilon_l. \quad (70)$$

Now, one can find the matrix elements as

$$\begin{aligned}
h_{11} &= \left\langle \varphi_{2s}(\mathbf{r} - \mathbf{t}_j) \middle| \mathbb{H} \middle| \varphi_{2s}(\mathbf{r} - \mathbf{t}_j) \right\rangle = \varepsilon_{2s}, \\
h_{ii} &= \left\langle \varphi_{2p_n}(\mathbf{r} - \mathbf{t}_j) \middle| \mathbb{H} \middle| \varphi_{2p_n}(\mathbf{r} - \mathbf{t}_j) \right\rangle = \varepsilon_{2p}, \\
i &= 2, 3, 4 \quad i = 2, n = x \\
&\quad i = 3, n = y \\
&\quad i = 4, n = z \\
h_{55} &= \left\langle \varphi_{1s}(\mathbf{r} - \mathbf{t}_j) \middle| \mathbb{H} \middle| \varphi_{1s}(\mathbf{r} - \mathbf{t}_j) \right\rangle = \varepsilon_{1s}.
\end{aligned} \tag{71}$$

The remaining terms h_{ij} with $i \neq j$ are zero. In tabular form H_{AA} is given by

$$H_{AA} = \begin{pmatrix} \varepsilon_{2s} & 0 & 0 & 0 & 0 \\ 0 & \varepsilon_{2p} & 0 & 0 & 0 \\ 0 & 0 & \varepsilon_{2p} & 0 & 0 \\ 0 & 0 & 0 & \varepsilon_{2p} & 0 \\ 0 & 0 & 0 & 0 & \varepsilon_{1s} \end{pmatrix}. \tag{72}$$

Suggested model parameters values fitted to the electronic band structure along the high-symmetry lines are $\varepsilon_{2s} = -5.2$ eV, $\varepsilon_{2p} = 2.3$ eV, and $\varepsilon_{1s} = -4$ eV.

Similarly, H_{AB} has the tabular form as

$$H_{AB} = \begin{pmatrix} h_{11} & h_{12} & h_{13} & h_{14} & h_{15} \\ h_{21} & h_{22} & h_{23} & h_{24} & h_{25} \\ h_{31} & h_{32} & h_{33} & h_{34} & h_{35} \\ h_{41} & h_{42} & h_{43} & h_{44} & h_{45} \\ h_{51} & h_{52} & h_{53} & h_{54} & h_{55} \end{pmatrix}. \tag{73}$$

The components of the H_{AB} have the general form of

$$h_{ji} = \left\langle \varphi_m(\mathbf{r} - \mathbf{t}_j) \middle| \mathbb{H} \middle| \varphi_l(\mathbf{r} - \mathbf{t}_i - \mathbf{R}) \right\rangle = \delta(\mathbf{t}_j - \mathbf{t}_i - \mathbf{R}) V_{lm,ij}. \tag{74}$$

Here, \mathbf{d} denotes the nearest neighbor atoms position. Thus, what remains is to determine the rest of four nearest neighbors vectors \mathbf{R}_{Ai} of each carbon atom shown in Figure IV.3.2.

We need to project these vectors to Cartesian coordinate. Figure IV.3.3 shows the tetrahedral structure constructed by the center carbon atom, denoted by the letter A, and its nearest neighbors.

The bonding length of two carbon atoms a_{C-C} is about 1.52 Å and the bonding length of carbon and hydrogen atoms a_{C-H} is about 1.1 Å. Also C-C-H angle θ is about 109.5°. Figure IV.3.4 shows the triangles constructed on A, B and C points and A, C and D points. Here β is the complementary of the angle θ , given by $\beta = \pi - \theta$. Using the triangular relations, one can get the distances h and w as well.

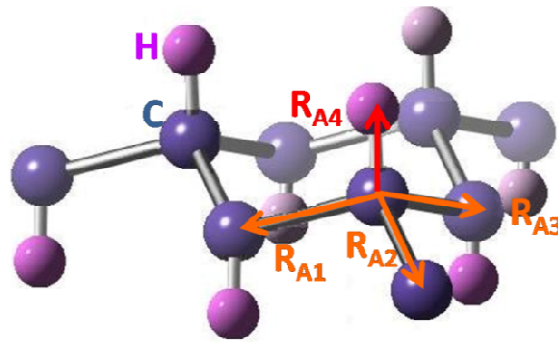


Figure IV.3.2. Four nearest neighbors of the carbon atom: three carbon and one hydrogen atoms.

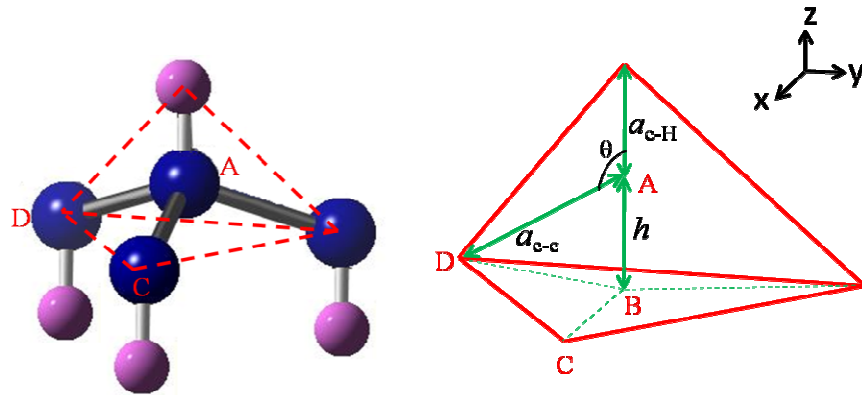


Figure IV.3.3. The tetrahedral structure constructed by atoms in graphane.

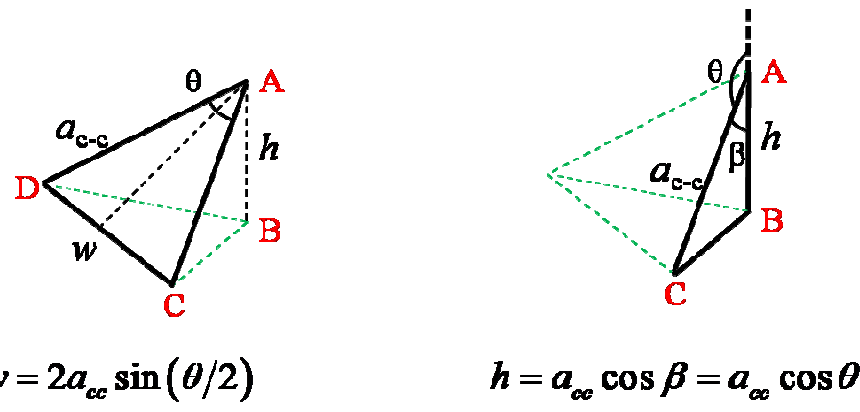


Figure IV.3.4. The triangles structure constructed to calculate h and w .

Now, suppose that the central carbon atom C_0 is located at the origin of the Cartesian coordinate. Using the recent calculated parameters, one can get the location of the nearest neighbors of the carbon atom A as

$$\begin{aligned} C_0 &: (0, 0, 0), \\ C_1 &: \left(\frac{w}{\sqrt{3}}, 0, -h \right), \\ C_2 &: \left(-\frac{w}{2\sqrt{3}}, \frac{w}{2}, -h \right), \\ C_3 &: \left(-\frac{w}{2\sqrt{3}}, -\frac{w}{2}, -h \right), \\ H &: (0, 0, a_{C-H}). \end{aligned} \quad (75)$$

Figure IV.3.5 shows the projected location of these atoms on xy -plane.

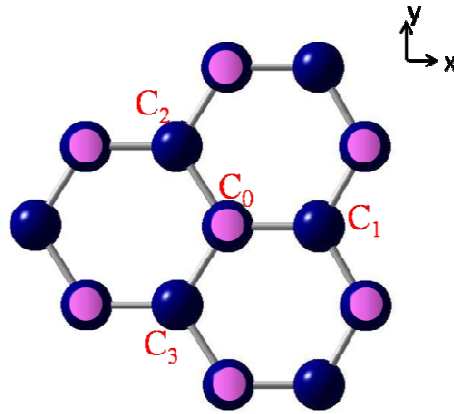


Figure IV.3.5. Top view of the atoms specified with (75).

Now, one can write \mathbf{R}_{Ai} vectors needed to calculate Hamiltonian parameters H_{AB} as

$$\begin{aligned} \mathbf{R}_{A1} &: \left(\frac{w}{\sqrt{3}}, 0, -h \right), \\ \mathbf{R}_{A2} &: \left(-\frac{w}{2\sqrt{3}}, \frac{w}{2}, -h \right), \\ \mathbf{R}_{A3} &: \left(-\frac{w}{2\sqrt{3}}, -\frac{w}{2}, -h \right), \\ \mathbf{R}_{A4} &: (0, 0, a_{C-H}). \end{aligned} \quad (76)$$

For each of the \mathbf{R}_{Ai} vectors, one can define the corresponding angles made with respect to the x , y and z axes as θ_x , θ_y and θ_z . Considering these vectors, the components of H_{AB} can be written out as

$$h_{11} = \langle \varphi_{A2s} | \mathbb{H} | \varphi_{B2s} \rangle = V_{ss\sigma} \sum_{i=1}^3 e^{i\mathbf{k} \cdot \mathbf{R}_{Ai}}, \quad (77)$$

$$h_{12} = \langle \varphi_{A2s} | \mathbb{H} | \varphi_{B2p_x} \rangle = V_{sp\sigma} \sum_{i=1}^3 \cos \theta_x e^{i\mathbf{k} \cdot \mathbf{R}_{Ai}}, \quad (78)$$

$$h_{13} = \langle \varphi_{A2s} | \mathbb{H} | \varphi_{B2p_y} \rangle = V_{sp\sigma} \sum_{i=1}^3 \cos \theta_y e^{i\mathbf{k} \cdot \mathbf{R}_{Ai}}, \quad (79)$$

$$h_{14} = \langle \varphi_{A2s} | \mathbb{H} | \varphi_{B2p_z} \rangle = V_{sp\sigma} \sum_{i=1}^3 \cos \theta_z e^{i\mathbf{k} \cdot \mathbf{R}_{Ai}}, \quad (80)$$

$$h_{15} = \langle \varphi_{A2s} | \mathbb{H} | \varphi_{H1s} \rangle = V_{1s1s} e^{i\mathbf{k} \cdot \mathbf{R}_{A4}}, \quad (81)$$

$$h_{22} = \langle \varphi_{A2p_x} | \mathbb{H} | \varphi_{B2p_x} \rangle = \sum_{i=1}^3 \left[V_{pp\sigma} \cos^2 \theta_x + V_{pp\pi} (1 - \cos^2 \theta_x) \right] e^{i\mathbf{k} \cdot \mathbf{R}_{Ai}}, \quad (82)$$

$$h_{23} = \langle \varphi_{A2p_x} | \mathbb{H} | \varphi_{B2p_y} \rangle = \sum_{i=1}^3 (V_{pp\sigma} - V_{pp\pi}) \cos \theta_x \cos \theta_y e^{i\mathbf{k} \cdot \mathbf{R}_{Ai}}, \quad (83)$$

$$h_{24} = \langle \varphi_{A2p_x} | \mathbb{H} | \varphi_{B2p_z} \rangle = \sum_{i=1}^3 (V_{pp\sigma} - V_{pp\pi}) \cos \theta_x \cos \theta_z e^{i\mathbf{k} \cdot \mathbf{R}_{Ai}}, \quad (84)$$

$$h_{33} = \langle \varphi_{A2p_y} | \mathbb{H} | \varphi_{B2p_y} \rangle = \sum_{i=1}^3 \left[V_{pp\sigma} \cos^2 \theta_y + V_{pp\pi} (1 - \cos^2 \theta_y) \right] e^{i\mathbf{k} \cdot \mathbf{R}_{Ai}}, \quad (85)$$

$$h_{34} = \langle \varphi_{A2p_y} | \mathbb{H} | \varphi_{B2p_z} \rangle = \sum_{i=1}^3 (V_{pp\sigma} - V_{pp\pi}) \cos \theta_y \cos \theta_z e^{i\mathbf{k} \cdot \mathbf{R}_{Ai}}, \quad (86)$$

$$h_{35} = \langle \varphi_{A2py} | \mathbb{H} | \varphi_{1s} \rangle = -V_{1s2p} \cos \theta_y e^{i\mathbf{k} \cdot \mathbf{R}_{A4}}, \quad (87)$$

$$h_{44} = \langle \varphi_{A2p_z} | \mathbb{H} | \varphi_{B2p_z} \rangle = \sum_{i=1}^3 \left[V_{pp\sigma} \cos^2 \theta_z + V_{pp\pi} (1 - \cos^2 \theta_z) \right] e^{i\mathbf{k} \cdot \mathbf{R}_{Ai}}, \quad (88)$$

$$h_{45} = \langle \varphi_{A2pz} | \mathbb{H} | \varphi_{1s} \rangle = -V_{1s2p} \cos \theta_z e^{i\mathbf{k} \cdot \mathbf{R}_{A4}}, \quad (89)$$

$$h_{55} = \langle \varphi_{H1s} | \mathbb{H} | \varphi_{H1s} \rangle = V_{1ss} e^{i\mathbf{k} \cdot \mathbf{R}_{A4}}. \quad (90)$$

Other parameters can be written based on the facts that $\langle s | \mathbb{H} | p \rangle = -\langle p | \mathbb{H} | s \rangle$, $\langle p_1 | \mathbb{H} | p_2 \rangle = \langle p_2 | \mathbb{H} | p_1 \rangle$ and $\langle s_1 | \mathbb{H} | s_2 \rangle = \langle s_2 | \mathbb{H} | s_1 \rangle$. We choose the model parameter values, fitted to the electronic band structure along the high-symmetry lines, to be $V_{sp\sigma} = 3.8\text{eV}$, $V_{ss\sigma} = -4.4\text{eV}$, $V_{pp\sigma} = 5.6\text{eV}$, $V_{pp\pi} = -1.8\text{eV}$, $V_{1s1s} = 0\text{eV}$, $V_{1s2p} = 4\text{eV}$, and $V_{1ss} = -3.5\text{eV}$. As mentioned before, the matrix element H_{AA} is exactly the same as H_{BB} and H_{AB} is simply the complex conjugate of H_{BA} .

Figure IV.3.6 shows the resultant electronic band structure of graphane obtained from direct Tight-binding calculations. The irreducible Brillouin zone is again the half of an equilateral triangle with apexes \varnothing , K and M, exactly like in graphene, as shown in Figure III.3.2.

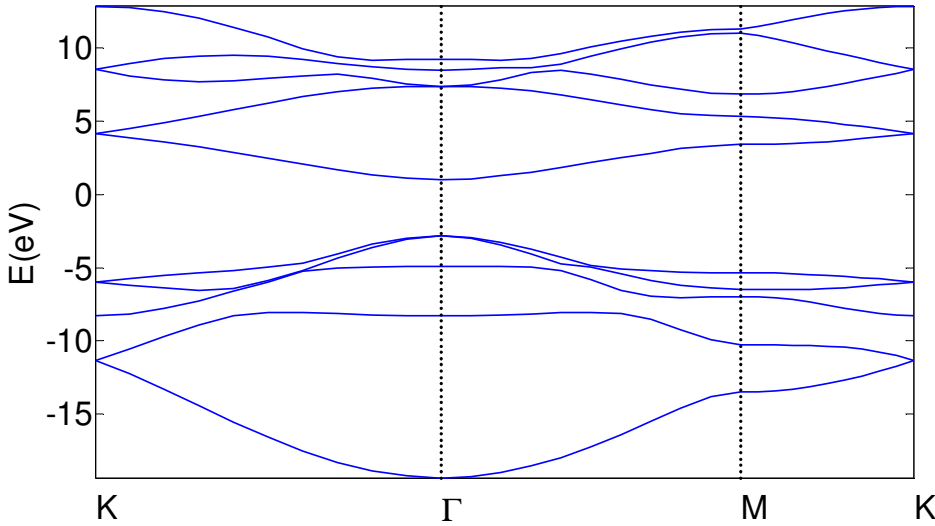


Figure IV.3.6. The top view of the atoms specified

There is an excellent agreement compared to the reported result in [39], which are obtained from density-functional theory calculations, as shown in Figure IV.3.7. This establishes the usefulness and high accuracy of the Tight-binding method as applied to the planar graphene and graphane structures. We here notice that the former structure is a semimetal with a zero-gap at its Dirac points, while the latter is a semiconductor with a direct energy gap.

Chemical functionalization is a viable route toward bandgap engineering of graphene-based materials, as first demonstrated in [40], where exposure to a stream of hydrogen atoms has led to 100% hydrogenation of a graphene sheet, the so-called graphane.

The band gap of periodically doped graphene with hydrogen is investigated. It is found through a Tight-binding model that for certain periodicities, called nongap periodicities (NGPs), no gap is opened at the Dirac point. Density-functional-theory calculations show that a tiny gap is opened for NGPs due to exchange effects, not taken into account in the TB model. However, this tiny gap is one order of magnitude smaller than the gap opened for other periodicities different from NGPs. This remarkable reduction in the band-gap opening for NGPs provokes a crossing of the midgap and the conduction bands and, consequently, the metallization of the system. This result is also valid for other adsorbates different from atomic hydrogen [51].

Although graphene is a gapless semimetal due to the symmetry between two sublattices of the honeycomb structure, graphane is a semiconductor with a wide bandgap around 3.5eV

[39]. This gives good idea for opening gap in Dirac points of graphene. Furthermore, it is possible to control the gap in graphane by removing some of its hydrogen atoms periodically [52, 53]. The role of hydrogen vacancies is to decrease the energy gap, and at the same time, to increase the thermoelectric figure of merit [54], as well as significant lattice contraction. It has been also noticed that such hydrogen vacancy clusters in graphane may appear as quantum dots and induction of stable ferromagnetism [55]. Furthermore, it has been shown that single-sided hydrogenation also causes reduction of energy gap to about 1.1eV [52].

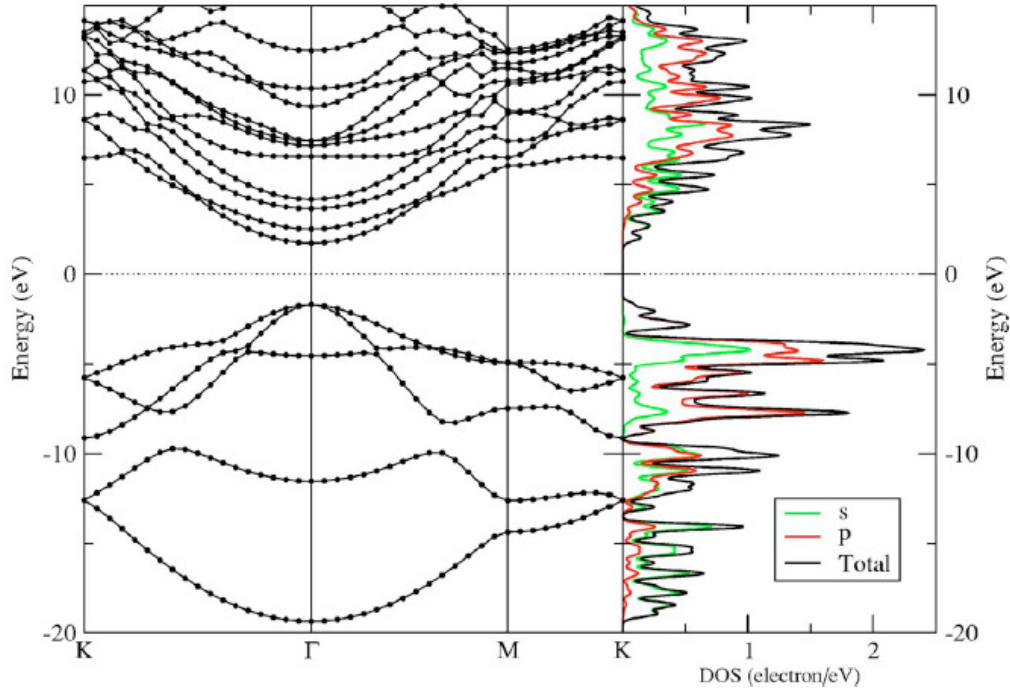


Figure IV.3.7. Band structure and density of states of graphane [40].

Obviously, research on functionalized graphane devices is at an embryonic stage. Several issues must be addressed to introduce graphane in future generations of electron devices. From this perspective, theoretical simulations have been done to explore possible solutions for device fabrication and design, in order to provide an early assessment of the opportunities of functionalized graphane in nanoscale electronics.

Together with the 2-D geometry and unique transport features of graphene, the possibility of doping graphane makes it possible to define p and n regions so that 2-D p-n junctions become feasible with small reverse currents. This junction is designed based on patterned graphane and its current-voltage characteristics is also predicted [52]. Experimental characteristics of such a junction is observed in [56]. Recent analysis also shows possibilities of designing bipolar junction transistors based on patterned graphane [57]. For this reason, donor and acceptor impurities should be introduced to the graphane with controlled concentrations, the effects of which have been also studied [58].

A performance analysis of field-effect transistors (FETs) based on recently fabricated 100% hydrogenated graphene (graphane) [55] and theoretically predicted semihydrogenated graphene (graphone) [59] has been also reported. The approach is based on accurate calculations of the energy bands by means of GW approximation, subsequently fitted with a three-nearest neighbor sp^3 tight-binding Hamiltonian, and finally used to compute ballistic transport in transistors based on functionalized graphene. Due to the large energy gap, the proposed devices have many of the advantages provided by one-dimensional graphene nanoribbon FETs, such as large I_{on} and I_{on}/I_{off} ratios, reduced band-to-band tunneling, without the corresponding disadvantages in terms of prohibitive lithography and patterning requirements for circuit integration [60]. Recent advances in the fabrication of graphene integrated circuits paves the way toward the expected birth of two-dimensional nanoscale planar electronics based on the graphene and graphane [61].

REFERENCES

- [1] Bloch, F. *Z. Phys.* 1928, vol. 52.
- [2] Slater, JC; Koster, GF. *Phys. Rev.* 1954, vol. 94, 1498.
- [3] Martin, RM. *Electronic Structure: Basic Theory and Practice Methods*, Cambridge University Press, 2004.
- [4] Kittel, C. *Introduction to Solid State Physics*, 7th ed., Wiley, 1996.
- [5] Ashcroft, NW; Mermin, ND. *InSolid State Physics*, Holt, Rinehart and Winston, New York, NY, 1976.
- [6] Sutton, AP. *Electronic Structure of Materials*, Oxford University Press, Oxford, UK, 1993.
- [7] Harrison, AW. *Structure and the Properties of Solids*, Dover, New York, 1989.
- [8] Saito, R; Dresselhaus, G; Dresselhaus, MS. *Physical Properties of Carbon Nanotubes*, Imperial, London, 1998.
- [9] Dresselhaus, MS; Dresselhaus, G; Sugihara, K; Spain, IL; Goldberg, HA. *Springer Series in Materials Science*, 1988, vol. 5.
- [10] Ravagnan, L; Mazza, T; Bongiorno, G; Devetta, M; Amati, M; Milani, P; Piseri, P; Coreno, M; Lenardi, C; Evangelista, F; Rudolf, P. *Chem. Commun.*, 2011, vol. 47, 2952.
- [11] Kaxiras, E; *Atomic and Electronic Structure of Solids*, Cambridge University Press, 2003.
- [12] Zhang, Q.; Chan, K. S.; Lin, Z.; *Appl. Phys. Lett.*, 2011, vol. 98, 032106.
- [13] Geim, AK; Novoselov, KS. *Nature Materials*, 2007, vol. 6, 183.
- [14] Pauling, L; *The Nature of the Chemical Bond*, Cornell U. P., Ithaca, NY, 1972.
- [15] Peres, NMR; Guinea, F; Castro Neto, AH. *Phys. Rev. B*, 2006, vol. 73, 125411.

- [16] Novoselov, KS. *Nature*, 2005, vol. 438, 197.
- [17] Abanin, DA; Lee, PA; and Levitov, LS. *Phys. Rev. Lett*, 2006, vol. 96, 176803.
- [18] http://nobelprize.org/nobel_prizes/physics/laureates/2010/
- [19] Gharekhani, B.; Alavi, M; Khorasani, S. *Semicond. Sci. Technol.*, 2008, vol. 23, no. 7, 075026.
- [20] Boukhvalov, DW; Katsnelson, MI.; Lichtenstein, A. I. *Phys. Rev. B*, 2008, vol. 77, 035427.
- [21] Peres, NMR.; Guinea, F; Castro Neto, AH. *Phys. Rev. B*, 2006, vol. 73, 125411.
- [22] Pereira, VM.; Guinea, F; Lopes dos Santos, JMB; Peres, NMR; Castro Neto, AH. *Phys. Rev. Lett*, 2006, vol. 96, 036801.
- [23] Vanin, M; Mortensen, JJ; Kelkkanen, AK; García-Lastra, JM; Thygesen, KS; Jacobsen, KW. *Phys. Rev. B*, 2010, vol. 81, 081408.
- [24] Lu, YH; Feng, YP. *J. Phys. Chem.*, 2009, C 113, 20841.
- [25] Han, MY; Ozyilmaz, B; Zhang, Y; Kim, P. *Phys. Rev. Lett*, 2007, vol. 98, 206805.
- [26] Son, YW; Cohen, ML; Louie, SG. *Phys. Rev. Lett*, 2006, vol. 97, 216803.
- [27] Pedersen, TG; Flindt, C; Pedersen, J; Mortensen, NA; Jauho, A-P; Pedersen, K. *Phys. Rev. Lett*, 2008, vol. 100, 136804.
- [28] Tiwari, RP; Stroud, D. *Phys. Rev. B*, 2009, vol. 79, 205435.
- [29] Liu, W; Wang, ZF; Shi, QW; Yang, J; Liu, F. *Phys. Rev. B*, 2009, vol. 80, 233405.
- [30] Bai, J; Zhong, X; Jiang, S; Huang, Y; Duan, X. *Nature Nanotech.*, 2010, vol. 5, 190.
- [31] Schultz, MH; Jauho, AP; Pedersen, TG. *Phys. Rev. B*, 2011, vol. 84, 045428.
- [32] Penga, J; Li, S. *App. Phys. Lett*, 2010, vol. 97, 242105.
- [33] Song, L; Ci, LJ; Lu, H; Sorokin, PB; Jin, CH; Ni, J; Kvashnin, AG; Kvashnin, DG; Lou, J; Yakobson, BI; Ajayan, PM. *Nano Lett.*, 2010, vol. 10, 3209.
- [34] Zhang, A; Teoh, HF; Dai, Z; Feng, YP; Zhang, C. *App. Phys. Lett*, 2011, vol. 98, 023105.
- [35] Balog, R; Jørgensen, B; Nilsson, L; Andersen, M; Rienks, E; Bianchi, M; Fanetti, M; Lægsgaard, E; Baraldi, A; Lizzit, S; Sljivancanin, Z; Besenbacher, F; Hammer, B; Pedersen, TG; Hofmann P; Hornekær, L. *Nature Materials*, 2010, vol. 9, 315.
- [36] Dreyer, RD; Park, S; WB, Christopher ; Ruoff, S. R. *Chem. Soc. Rev.*, 2010, vol. 39, 228.
- [37] Kovtyukhova, N I; Karpenko, GA; Chuiko, AA. *Russ. J. Inorg. Chem.* 1992, vol. 37, 566.
- [38] Liu, P; Gong, K; Xiao, P. *Carbon*, 1999, vol. 37, 2073.
- [39] Sofo, JO; Chaudhari, AS; Barber; GD. *Phys. Rev. B*, 2007, vol. 75, 153401.

- [40] Elias, DC; Nair, RR; Mohiuddin, TMG; Morozov, SV; Blake, P; Halsall, MP; Ferrari, AC; Boukhvalov, DW; Katsnelson, MI; Geim, AK; Novoselov, KS. *Science*, 2009, vol. 323, 610.
- [41] Jones, JD; Hoffmann, WD; Jesseph, AV; Morris, CJ; Verbeck, GF; Perez, J. M. *App. Phys. Lett.*, 2010, vol. 97, 233104.
- [42] Bhattacharya, A.; Bhattacharya, S.; Majumder, C.; Das, G. P. *Phys. Rev. B*, 2011, vol. 83, 033404.
- [43] Cadelano, E; Palla, PL; Giordano, S; Colombo, L. *Phys. Rev. B*, 2010, vol. 82, 235414.
- [44] Neek-Amal, M; Peeters, FM. *Phys. Rev. B*, 2011, vol. 83, 235437.
- [45] Ijäs, M; Havu, P; Harju, A; Pasanen, P. *Phys. Rev. B*, 2011, vol. 84, 041403(R).
- [46] Averill, FW; Morris, JR; *Phys. Rev. B*, 2011, vol. 84, 035411.
- [47] Savini, G; Ferrari, AC; Giustino, F. *Phys. Rev. Lett.*, 2011, vol. 105, 037002.
- [48] Kristoffel, N; Rägo, K. *Phys. Lett. A*, 2011, vol. 375, 2246.
- [49] Loktev, VM; Turkowski, V; *J. Low Temp. Phys.*, 2011, vol. 164, 264.
- [50] Boukhvalov, DW; Katsnelson, MI; Lichtenstein, A. I. *Phys. Rev. B*, 2008, vol. 77, 035427.
- [51] García-Lastra, J. M. *Phys. Rev. B*, 2010, vol. 82, 235418.
- [52] Gharekhanlou, B; Khorasani, S. *IEEE Trans. Electron Dev.*, 2010, vol. 57, 209.
- [53] Savchenko, A. *Science*, 2009, vol. 323, 589.
- [54] Ni, X; Liang, G; Wang, J-S; Li, B. *App. Phys. Lett.*, 2009, vol. 95, 192114.
- [55] Singh, AK; Penev ES; Yakobson, BI. *ACS Nano*, 2010, vol. 4, 3510.
- [56] Courtesy of N. Ranjan-Ray (Saha Institute, India) private communication.
- [57] Gharekhanlou, B; Tousaki, SB; Khorasani, S. *J. Phys.: Conf. Series*, 2010, vol. 248, 012061.
- [58] Wang, Y; Ding, Y; Shi, S; Tang, W. *Appl. Phys. Lett.*, 2011, vol. 98, 163104.
- [59] Pujari, BS; Gusarov, S; Brett, M; Kovalenko, A; *Phys. Rev. B*, 2011, vol. 84, 041402(R).
- [60] Fiori, G; Lebègue, S; Betti, A; Michetti, P; Klintenberg, M; Eriksson, O; Iannaccone, G. *Phys. Rev. B*, 2010, vol. 82, 153404.
- [61] Lin, YM; Valdes-Garcia, A; Han, SJ; Farmer, DB; Meric, I; Sun, Y; Wu, Y; Dimitrakopoulos, C; Grill, A; Avouris, P; Jenkins, KA. *Science*, 2011, vol. 332, 1294.